The North Atlantic Glacial Eastern Boundary Current as a Key Driver for Ice-Sheet-AMOC Interactions and Climate Instability

Samuel Toucanne, Guillaume Soulet, Natalia Vázquez Riveiros, Steven Boswell, Bernard Dennielou, Claire Waelbroeck, Germain Bayon, Meryem Mojtahid, Mathieu Bosq, Marjolaine Sabine, et al.

HAL Id: hal-03434827
https://hal.science/hal-03434827

Submitted on 19 Nov 2021

The North Atlantic Glacial Eastern Boundary Current as a Key Driver for Ice-Sheet—AMOC Interactions and Climate Instability

Samuel Toucanne[1] , **Guillaume Soulet**[1] , **Natalia Vázquez Riveiros**[1] , **Steven M. Boswell**[2] , **Bernard Dennielou**[1] , **Claire Waelbroeck**[3] , **Germain Bayon**[1] , **Meryem Mojtahid**[4] , **Mathieu Bosq**[5] , **Marjolaine Sabine**[6], **Sébastien Zaragosi**[6] , **Jean-François Bourillet**[1] , and **Herlé Mercier**[7]

[1]IFREMER, Unité de Recherche Géosciences Marines, Laboratoire Géophysique et enregistrement Sédimentaire, Plouzané, France, [2]Lamont-Doherty Earth Observatory, Columbia University, Palisades, NY, USA, [3]Laboratoire d'Océanographie et du Climat: Expérimentation et Approches Numériques, LOCEAN/IPSL, Sorbonne Université-CNRS-IRD-MNHN, UMR7159, Paris, France, [4]LPG-BIAF UMR-CNRS 6112, Université d'Angers, UFR Sciences, Angers Cedex, France, [5]PACEA, UMR 5199 CNRS - Université Bordeaux, Pessac, France, [6]UMR-CNRS 5805 EPOC - OASU, Université de Bordeaux, Pessac, France, [7]CNRS, IFREMER, Université de Brest, IRD, Laboratoire d'Océanographie Physique et Spatiale (LOPS), Centre IFREMER de Bretagne, Plouzané, France

Abstract The upper branch of the Atlantic meridional overturning circulation (AMOC) plays a critical role in ocean circulation and climate change, yet its variability during the last glacial period is poorly documented. Here, we investigate the northward-flowing Glacial Eastern Boundary Current (GEBC) in the North Atlantic, known today as the European Slope Current, and representing the easternmost portion of the upper branch of the AMOC. Based on flow speed and isotopic records, we show that Dansgaard-Oeschger (D-O) interstadials (stadials) correspond to a faster (weaker) GEBC during the ~50–15 ka period. This, by analogy to present-day conditions, suggests enhanced (reduced) strength of the subpolar gyre and, by extension, of northern-sourced water production and AMOC during D-O interstadials (stadials). Concomitant fluctuations of both the GEBC and the European Ice Sheet between ~30 and 17 ka suggest an active role of the upper branch of AMOC in the poleward transport of heat and freshwater to the northern North Atlantic, with direct impacts on deep water formation and AMOC strength. We explore these ice-sheet—AMOC interactions and the associated abrupt climate changes over the last glacial period and the last deglaciation.

1. Introduction

The Atlantic meridional overturning circulation (AMOC), consisting of a warm, northward flow in the upper layer of the Atlantic, the formation of North Atlantic Deep Water (NADW) at high latitudes, and southward return flow at depth, moves immense amounts of heat northwards (Hall & Bryden, 1982; Trenberth et al., 2019). Ocean circulation is thus an active player in the global climate system. A causal link has been proposed between changes in the AMOC and the climate swings of the last glacial cycle (Broecker, 1991; Broecker & Denton, 1990; Lynch-Stieglitz, 2017; Rahmstorf, 2002). While this was first shown for the late-glacial period (Boyle & Keigwin, 1987; Lehman & Keigwin, 1992; Marchitto et al., 1998; McManus et al., 2004), the association between millennial-scale climate changes punctuating the last glacial cycle, that is, Dansgaard-Oeschger (D-O) oscillations (Dansgaard et al., 1993), and AMOC perturbations (Elliot et al., 2002; Keigwin & Jones, 1994) was studied at high resolution only recently (Böhm et al., 2015; Gottschalk et al., 2015; Henry et al., 2016; Hoogakker et al., 2007; Kissel et al., 2008; Waelbroeck et al., 2018). In brief, the AMOC in the deep North Atlantic was significantly weakened during the coldest intervals (stadials), whereas rapid accelerations were concurrent with Greenland and North Atlantic warm events (interstadials). This oceanic process is thought to have played a crucial role in the interhemispheric redistribution of heat and the asynchronous relationship observed between millennial-scale temperature changes over Greenland and Antarctica (Buizert, Keisling, et al., 2018; Buizert, Sigl, et al., 2018; EPICA Community Members, 2006; WAIS Divide Project Members, 2015).

Table 1
Core Locations

| Core label	Lat. N	Long. W	Depth (m)	Cruise (year)	IGSN
MD99-2328	48°04.62	9°30.35	942	IMAGES V LEG 4-MD114 (1999)	BFBGX-93178
CBT-CS10	47°31.83	7°29.455	1,015	CABTEX (2010)	BFBGX-86847
MD95-2002	47°27.12	8°32.03	2174	IMAGE1-MD101 (1995)	IEFRA05KC
BOB-CS03	47°23.665	6°45.041	1,011	BOBGEO (2009)	BFBGX-88574
GIT-CS02	47°21.83	6°44.92	1,051	GITAN (2015)	BFBGX-127464
BOB-CS05	46°18.85	4°38.12	1,015	BOBGEO (2009)	BFBGX-88576
MD04-2842	46°04.02	4°42.81	2,450	MD142-ALIENOR 2 (2004)	IEFRA04P1

Note. See Figure S1 for high-resolution bathymetric maps.

While there is currently little doubt that AMOC changes play a major role in the dynamics of the D-O oscillations, the causes and mechanisms behind these climatic events as well as their link to the episodic iceberg-discharge events (or Heinrich events, HE) from the Hudson Strait Ice Stream of the Laurentide Ice Sheet (LIS; Hemming, 2004) remain a subject of active discussion (see Menviel et al., 2020 for a review). Among the various processes invoked for D-O oscillations are the interactions between convection sites and the cryosphere in the North Atlantic, either through wind-stress forcing (Arzel et al., 2010; Wunsch, 2006; Zhang et al., 2014), sea-ice variability (Dokken et al., 2013; Gildor & Tziperman, 2003; Li et al, 2005, 2010; Sévellec & Fedorov, 2015), ice shelf collapse (Boers et al., 2018; Petersen et al., 2013), or meltwater fluxes (Broecker et al., 1990; Ganopolski & Rahmstorf, 2001; Manabe & Stouffer, 1995; Menviel et al., 2014), together with the reorganization of the ocean-atmosphere system in the Southern Hemisphere via changes in the ocean surface temperature, the position of the mid-latitude westerly winds and changes in ocean stratification and air-sea CO_2 fluxes (Buizert, Sigl, et al., 2018; Zhang et al., 2017). Numerical approaches underscore the fundamental role of heat and salt in the millennial scale AMOC changes, revealing that their northward transport by the Gulf Stream—North Atlantic Current (NAC) system sustains internal feedbacks and oscillations (Arzel et al., 2010; Boers et al., 2018; Peltier & Vettoretti, 2014; Saha, 2015; Shaffer et al., 2004; Webb et al., 1997). This highlights the role of the upper branch of the AMOC in glacial millennial-scale climate fluctuations (Chapman & Shackleton, 1998; Lehman & Keigwin, 1992; Rasmussen & Thomsen, 2004).

The glacial variability of the upper branch of the AMOC remains poorly documented. Although some records have been successfully obtained from the western (sub)tropical Atlantic where the Gulf Stream originates (Hoogakker et al., 2013; Lynch-Stieglitz et al., 1999, 2014; Vautravers et al., 2004) to the northern end of the NAC in the Nordic Seas (Lehman & Keigwin, 1992; Rasmussen & Thomsen, 2004, 2008; Weinelt et al., 2003), direct evidence for millennial-scale changes in the vigor of the upper branch of the AMOC has yet to emerge. Here we provide inferred flow speed records from the upper slope (∼1,000 m) of the French Atlantic margin that display clear D-O variability. This result, together with oxygen, carbon and radiogenic neodymium isotopic data, reflects the variability of the northward-flowing eastern boundary current along the western European margin, known today as the European Slope Current and constituting the easternmost portion of the upper branch of the AMOC (Huthnance et al., 2020). We explore the role of this current in ice-sheet—AMOC interactions and glacial abrupt climate shifts.

2. Core Location and Hydrographic Setting

This study is based on six long-piston cores from the French Atlantic margin, located along a 450 km-transect between 46°N and 48°N (Table 1, Figure 1 and Figure S1). Five of these cores (MD99-2328, CBT-CS10, BOB-CS03, GIT-CS02, and BOB-CS05) were retrieved at ∼1,000 m water depth in the upper slope to produce a continuous composite stratigraphic record (see Section 4). Core MD04-2842 was retrieved at 2,450 m. Lithofacies at these intermediate depth sites consist of muddy to fine-sandy contourites (see Text S1; Stow & Holbrook, 1984), that is, sediments deposited or substantially reworked by the persistent action (e.g., selective deposition, winnowing, erosion) of bottom currents.
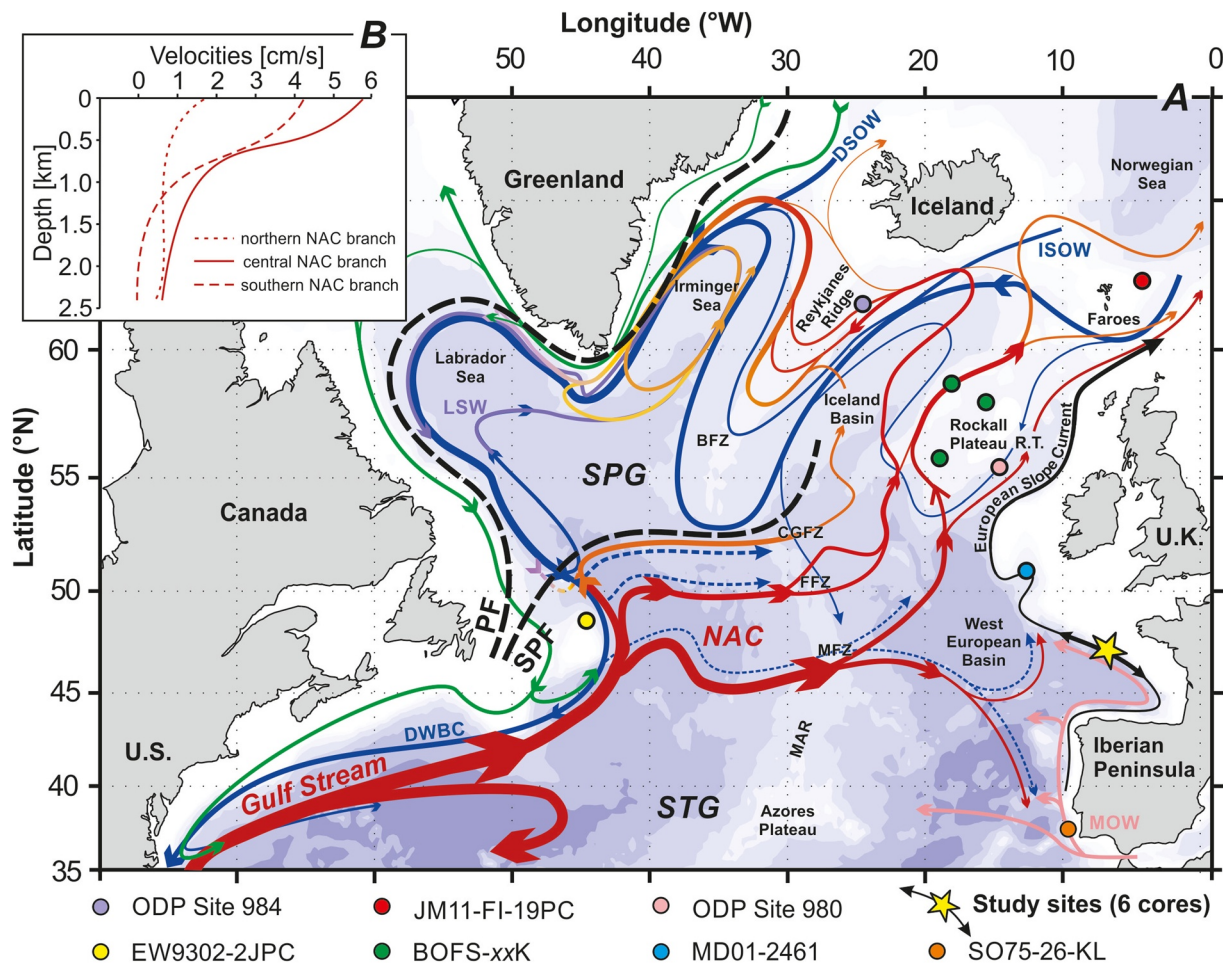
Figure 1. The modern North Atlantic Ocean circulation. (a) Detailed schematic of the upper cell of the AMOC with a warm, northward flow in the upper Atlantic (Gulf-Stream—North Atlantic Current (NAC) system, upper branch of the AMOC; red arrows), the formation of North Atlantic Deep Water (NADW) at high latitudes (i.e., DSOW, ISOW, and LSW; see below), and southward return flow (lower branch of the AMOC; blue arrows) at depth (including the Deep Western Boundary Current, DWBC). The main water masses are indicated: Denmark Strait Overflow Water (DSOW), Iceland-Scotland Overflow Water (ISOW), Labrador Sea Water (LSW) and Mediterranean Outflow Water (MOW). Dashed blue arrows highlight eastward recirculation of NADW by interior pathways. The European Slope Current (∼500–2,000 m along the European margin, black arrow), the Greenland currents (in green) and the polar (PF) and subpolar (SPF) fronts (dashed black lines) are shown. SPG: subpolar gyre. STG: subtropical gyre. The main topographical features controlling the flow pathways are labeled: Bight Fracture Zone (BFZ), Charlie–Gibbs Fracture Zone (CGFZ), Faraday Fracture Zone (FFZ), Maxwell Fracture Zone (MFZ), Mid-Atlantic Ridge (MAR), and Rockall Trough (RT). Color changes in the bathymetry at 100 m, at 1,000 m, and every 1,000 m below 1,000 m. Colored circles show the location of the core sites/records discussed in this study, including those from the French Atlantic margin (yellow star; Figure S1) (adapted from Daniault et al., 2016). (b) Averaged velocity (cm/s) profiles for the NAC branches (Daniault et al., 2016).

The modern hydrography of the mid-latitude NE Atlantic at intermediate depth is dominated by the presence of the Mediterranean Outflow Water (MOW) and the Labrador Sea Water (LSW) (Van Aken, 2000). The MOW is the main intermediate (∼600–1,500 m) water mass up to about 50°N (Iorga & Lozier, 1999), and overlies the LSW centered at ∼2,000 m (Van Aken, 2000). The distribution of these water masses, and in particular the MOW north of 48–50°N (Iorga & Lozier, 1999; Lozier & Stewart, 2008), is strongly impacted by an eastern boundary current, namely the European Slope Current (Booth & Ellett, 1983; Huthnance, 1986; Pingree & Le Cann, 1989) (Figure 1). This poleward along-slope current (or "contour" current because it flows along the bathymetric contours) is recognized down to ∼2,000 m from the Iberian margin (∼40°N) to the Faroe-Shetland Channel (∼60°N) where it forms, together with the NAC, the Norwegian Atlantic Slope Current (Orvik & Niiler, 2002). Mean velocities of the European Slope Current reach a maximum on the upper slope (∼500–1,000 m) and significantly increase poleward (Huthnance, 1986), from 5–10 cm.s^{-1} in the Bay of Biscay to 10–20 cm.s^{-1} along and north of the Hebridean slope (Pingree & Le Cann, 1989, 1990; Xu et al., 2015). Peak poleward flows (with velocities of up to 20–30 cm.s^{-1}) are observed in winter (Pingree

et al., 1999). Seasonal difference in current speed amount to ∼8–10 cm.s^{-1} on the Hebridean slope but only ∼5 cm.s^{-1} on the Bay of Biscay slopes (Xu et al., 2015). The European Slope Current controls the entrainment and dispersion of the suspended particulate matter and governs the slope sedimentation (de Madron et al., 1999; McCave et al., 2001; Thomsen & Van Weering, 1998). This is supported at geological timescale by the occurrence of thick continental slope contourite deposits all along the western European margin (Hernández-Molina et al., 2011; Laberg et al., 2005).

The European Slope Current is driven both by the steep topography of the European margin and large-scale meridional density gradients (Friocourt et al., 2007, 2008; Huthnance, 1984; Pingree & Le Cann, 1990). Recent observations from the Hebridean region reveal that decadal scale variability in the strength of the European Slope Current is, to first order, directly connected to that of the cyclonic subpolar gyre (SPG; and associated meridional density gradients) with a strong (weak) SPG associated with a strong (weak) slope current (Marsh et al., 2017). These observations support the idea that the European Slope Current is largely recruited from the eastern North Atlantic and is connected, north of ∼55°N (i.e., Rockall Trough), to the upper part of the NAC (the NAC being the eastern limb of the SPG) (Houpert et al., 2020; Lozier et al., 2019). Further south, in the central North Atlantic (∼46–53°N), the NAC flows eastward in three main branches with circulation pathways strongly constrained by the Mid-Atlantic Ridge (MAR) (Daniault et al., 2016). The top-to-bottom transport of the NAC (down to 3,000–4,000 m water depth) east of the MAR is estimated at 41.8 ± 3.7 Sv, and ∼8–10 Sv are directly carried to the Nordic Seas by the southern NAC branch (Daniault et al., 2016; Lozier et al., 2019; Sarafanov et al., 2012). Along that route, the NAC impinges on the western European margin (as deep as 1,200 m; Lozier et al., 2019) and the Rockall Plateau subdivides the NAC in two quasi-permanent jets (Houpert et al., 2018). Then, the NAC branch in the Rockall Trough moves northward joining the European Slope Current that contributes about 2.7 ± 0.5 Sv (∼25%) to the Atlantic inflow entering the Nordic Seas (Berx et al., 2013). This warm, salty water forms the bulk of the upper branch of the AMOC (Huthnance et al., 2020; Lozier et al., 2019), compensating the dense overflows from the Nordic Seas that significantly contribute, together with LSW, to NADW (down to ∼4,500 m at ∼50°N) (Dickson & Brown, 1994; Lozier et al., 2019). The NADW is a major component of the global thermohaline circulation since it is the deep return flow (lower branch) of the "upper cell" of the AMOC (the deeper "lower cell" originates from Antarctica); the Deep Western Boundary Current (DWBC) along the eastern continental margin of North America is the primary export pathway of NADW at present (Buckley & Marshall, 2016). Recirculation of NADW by interior pathways (including LSW spreading toward the NE Atlantic; Bower et al., 2009) are signatures of interaction with the Gulf Stream—NAC system (Buckley & Marshall, 2016; Zou et al., 2017) (Figure 1).

Although the upper cell of AMOC was also present during the last glacial period (Pöppelmeier et al., 2020; Weber et al., 2007), the AMOC was possibly weaker (Du et al., 2020; Vettoretti & Peltier, 2013; Weber et al., 2007) and its geometry in the North Atlantic was likely shifted southward due to the presence of thick continental ice-sheets that altered wind patterns (Keffer et al., 1988; Löfverström et al., 2014). NADW was likely replaced by shallower (≤2,000 m), Northern-sourced intermediate-deep Waters (NSW; Boyle & Keigwin, 1987; Curry & Oppo, 2005; Duplessy et al., 1988; Lippold et al., 2012; Lynch-Stieglitz et al., 2007; Marchitto & Broecker, 2006; Oppo & Lehman, 1993; Sarnthein et al., 1994). The location of NSW convection sites (including that of the Glacial North Atlantic Intermediate Waters at the Last Glacial Maximum [LGM], ca. 26–19 ka; Boyle & Keigwin, 1987) remains uncertain. Nevertheless, it has been suggested that a shift from convection in the Nordic Seas (warm periods) to the subpolar open North Atlantic Ocean south of Iceland (cold periods) accompanied past climate changes at both glacial-interglacial (Duplessy et al., 1988; Ganopolski et al., 1998; Sarnthein et al., 1994) and D-O timescales (Ganopolski & Rahmstorf, 2001; Rahmstorf, 2002).

3. Methods

### 3.1. Near-Bottom Flow Speed: Sortable Silt and XRF Zr/Rb Ratio

Grain-size analyses (n = 1,055) were performed using a Mastersizer 3,000 laser diffraction particle size analyzer coupled to a Hydro LV wet dispersant unit after removal of sediment carbonate fraction with 1 N acetic acid. The "sortable silt" mean size ($\overline{SS}$), that is the mean grain size of the carbonate-free 10–63 μm
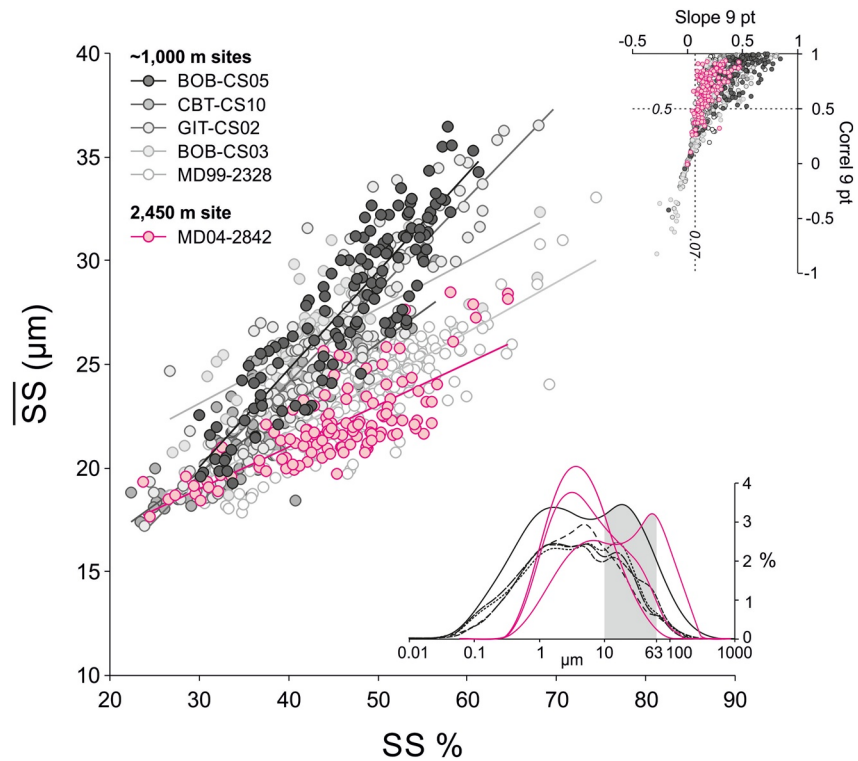
Figure 2. Sortable silt proxy validation. Dispersion plots of sortable silt (carbonate free, 10–63 μm silt fraction) mean size ($\overline{SS}$) versus percentage of sortable silt (SS%, in the total <63 μm terrigenous fraction) for the upper (~1,000 m water depth; gray and black circles) and middepth (2,450 m; magenta circles) French Atlantic contourites. The $\overline{SS}$—SS% data shown ($n = 794$) have both a running downcore correlation (R_{run}; nine-point) >0.5 and a slope >0.07 (upper right panel), which demonstrates that the sorting process is controlled by current flow dynamics (McCave & Andrews, 2019). Also shown are the grain size distributions for representative samples of contourite sediments (lower right panel) at ~1,000 m (black lines) and 2,450 m (magenta lines), with the 10–63 μm fraction highlighted in light gray.

terrigenous silt fraction, and the percentage of sortable silt (SS%) in the total <63 μm terrigenous fraction (McCave, Manighetti, & Beveridge, 1995), were calculated for each core (Figures 2 and 3). The $\overline{SS}$ provides a direct constraint on the rate of past bottom flows based on the principle that stronger currents yield a coarser mean size of the non-cohesive silt fraction (McCave & Andrews, 2019; McCave, Manighetti, & Robinson, 1995; McCave et al., 2017). The $\overline{SS}$ proxy is not sensitive to ice-rafted debris (IRD) inputs as long as this fraction is not >50% (McCave & Andrews, 2019). Our approach was complemented (for Marine Isotope Stage [MIS] 3, ~50–30 kyr BP) by using the XRF Zr/Rb ratio, a semi-quantitative grain-size indicator (Dypvik & Harris, 2001; Rothwell & Croudace, 2015) used in marine (Wu et al., 2020), lacustrine (Kylander et al., 2011), and terrestrial environments (Chen et al., 2006). In contourite deposits, XRF Zr/Rb provides a qualitative record of past changes in near-bottom current flow speed, since coarser grain size and stronger bottom currents are identified by a higher proportion of Zr-rich silt and sand (i.e., reflecting the presence of zircon grains) over Rb-rich clay (e.g., Toyos et al., 2020). Relative abundances of Zr and Rb, as well as those of major elements including Ca and Ti (see Section 4), were analyzed using an Avaatech X-ray Fluorescence (XRF) core scanner. XRF data were collected every 1 cm along the entire length of the cores with a counting time of 10 s, setting the voltage to 10 kV (no filter) and 30 kV (Pd thick filter) and the intensity to 600 and 1,000 μA, respectively. In addition, the lower part of core BOB-CS03 was analyzed every 1 mm (count time of 30 s, voltage of 10–30 kV, and intensity of 1,000 μA). Results are presented in log ratios of element intensities (Weltje & Tjallingii, 2008).
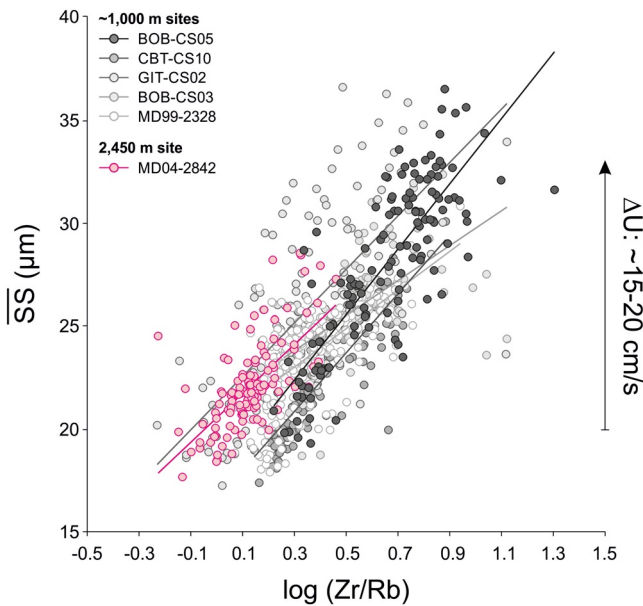
Figure 3. Grain-size proxies and related flow speed. Dispersion plots of $\overline{SS}$ versus log (Zr/Rb) ($n = 794$) for the upper (~1,000 m; gray and black circles) and middepth (2,450 m; magenta circles) French Atlantic contourites. Positive correlations ($0.65 < r < 0.85$) confirm the Zr/Rb ratio as a grain-size indicator (Dypvik & Harris, 2001; Rothwell & Croudace, 2015). The magnitude of *absolute changes* in flow speed (U) is given using a sensitivity of 1.36 ± 0.19 cm s^{-1}/µm (McCave et al., 2017).

3.2. Bottom-Water Chemistry: Carbon, Oxygen, and Radiogenic Neodymium Isotopes

Benthic foraminiferal ($n = 684$) $^{18}O/^{16}O$ and $^{13}C/^{12}C$ ratios ($\delta^{18}O$ and $\delta^{13}C$ respectively, expressed in ‰ with respect to the Vienna Pee-Dee Belemnite standard, VPDB) were measured to reconstruct changes in bottom water properties. Benthic $\delta^{18}O$ records combine bottom water $\delta^{18}O$ and temperature changes, whereas epibenthic foraminiferal $\delta^{13}C$ records changes in bottom water ventilation, defined as the transmission of oxygen-rich, atmosphere-equilibrated water to the ocean interior (Duplessy et al., 1988; Eide et al., 2017). Measurements were performed at the Laboratoire des Sciences de l'Environnement et du Climat (LSCE) and at the University of Bordeaux (UMR CNRS 5805 EPOC) on Elementar Isoprime and Optima Micromass mass spectrometers. VPDB is defined with respect to NBS-19 calcite standard ($\delta^{18}O = -2.20$‰ and $\delta^{13}C = +1.95$‰). The mean external reproducibility (1σ) of carbonate standards is ±0.05‰ for $\delta^{18}O$ and ±0.03‰ for $\delta^{13}C$. Measured NBS-18 $\delta^{18}O$ and $\delta^{13}C$ are -23.27 ± 0.10‰ VPDB and -5.01 ± 0.03‰ VPDB, respectively. Measurements were performed on *Cibicidoides kullenbergi* ($n = 481$), *Cibicidoides pachyderma* ($n = 118$), and *Cibicides wuellerstorfi* ($n = 53$) found in the 250–400 µm size fraction. The samples were cleaned in a methanol ultrasonic bath for a few seconds in order to remove impurities. A correction factor of $+0.34 \pm 0.03$‰ for $\delta^{13}C$ (calculated based on 21 paired analyses of *C. kullenbergi* and *C. wuellerstorfi*) was applied to the $\delta^{13}C$ values of *C. kullenbergi* and *C. pachyderma* to account for the relatively constant offset (linked to vital effect and/or habitat preferences) with regard to *C. wuellerstorfi* (Figure S2) that is believed to calcify in equilibrium with the isotopic composition of bottom-waters. No offset is apparent for $\delta^{18}O$ values (0.07 ± 0.26‰). Only 32 isotopic analyses (*C. wuellerstorfi*) were carried out on core MD04-2842 due to the scarcity of benthic foraminifera.

Radiogenic neodymium isotopic signatures (ε_{Nd}) of planktonic foraminifera coatings ($n = 70$) were used to investigate past changes in the provenance of bottom-water masses. Prior to Nd isotopic measurements, foraminiferal samples were prepared and dissolved following the method described in Tachikawa et al. (2014). Briefly, between ~6 and 21 mg of foraminifera were gently crushed between glass plates, then cleaned several times in ultrapure (18.2 MΩ) water in order to remove any detrital particles. The test fragments were transferred into acid-cleaned centrifuge tubes, covered with 500 µL ultrapure water, and dissolved progressively by stepwise addition (100 µL) of diluted (1 M) ultrapure glacial acetic acid solution. Nd was isolated using conventional ion chromatography and isotopic measurements were performed at the Pôle Spectrométrie Océan (Brest) using a Thermo Scientific Neptune multi-collector ICPMS. Nd isotopic compositions were determined using sample-standard bracketing by analyzing an in-house (SPEX-Nd) standard solution every two samples. Analyses of JNdi-1 standard solutions during the course of this study gave $^{143}Nd/^{144}Nd$ of 0.512117 ± 0.000009 (2 SD, $n = 10$), in agreement with the recommended value (0.512115) reported in Tanaka et al. (2000), and corresponding to an external reproducibility of ~±0.17ε (2 SD). Epsilon Nd values (ε_{Nd}) were calculated using the chondritic (CHUR) $^{143}Nd/^{144}Nd$ value of 0.512630 (Bouvier et al., 2008).

4. Chronology

The chronology of all studied cores is based on the synchronization of XRF data with that of the reference core MD95-2002 (Grousset et al., 2000; Toucanne et al., 2015; Figure S3), located at a maximum distance of ~450 km from the studied cores. The chronostratigraphy of core MD95-2002 is based on 26 ^{14}C ages (performed on monospecific *Globigerina bulloides* or *Neogloboquadrina pachyderma* samples) and additional control-points obtained through aligning both *N. pachyderma* abundances and XRF log (Ca/Ti) ratios to the NGRIP $\delta^{18}O$ record (GICC05 timescale; Table S1). The final age model of core MD95-

2002, extended here to ∼50 ka (∼38 ka in Toucanne et al., 2015), was established using the age modeling software Clam (Blaauw, 2010) and is reported with 95% confidence intervals (see Toucanne et al., 2015 for details).

Site-to-site stratigraphic correlations rely on the recognition of millennial-scale features (e.g. LGM-*n*, HS1-*n*, etc.) in the highly resolved XRF log (Ca/Ti) records (Figure S4 and Table S2). This approach revealed sediment hiatuses on the upper slope, especially for the late glacial-Holocene (Mojtahid et al., 2017) and MIS 3 (only recorded at site BOB-CS03) intervals (Figure S3). Nevertheless, the available time series allowed the production of a stratigraphic "composite" sequence at ∼1,000 m covering the last 48 kyr with the exception of the Bølling-Allerød interval that corresponds to a hiatus of sedimentation at all sites. In contrast, the deeper (mid-slope) core MD04-2842 shows a continuous stratigraphic sequence. Our chronologies reveal high mean sedimentation rates ranging from ∼30 cm.kyr^{-1} (cores BOB-CS03, MD04-2842) to ∼70 cm.kyr^{-1} (cores BOB-CS05, CBT-CS10) over the last glacial period and a high variability through time (e.g. ∼20 and 60 cm.kyr^{-1} in core BOB-CS03 for MIS 3 and MIS 2, respectively). Maximum sedimentation rates (∼100 cm. kyr^{-1}) are found at site MD99-2328 (Figure S5).

5. Results

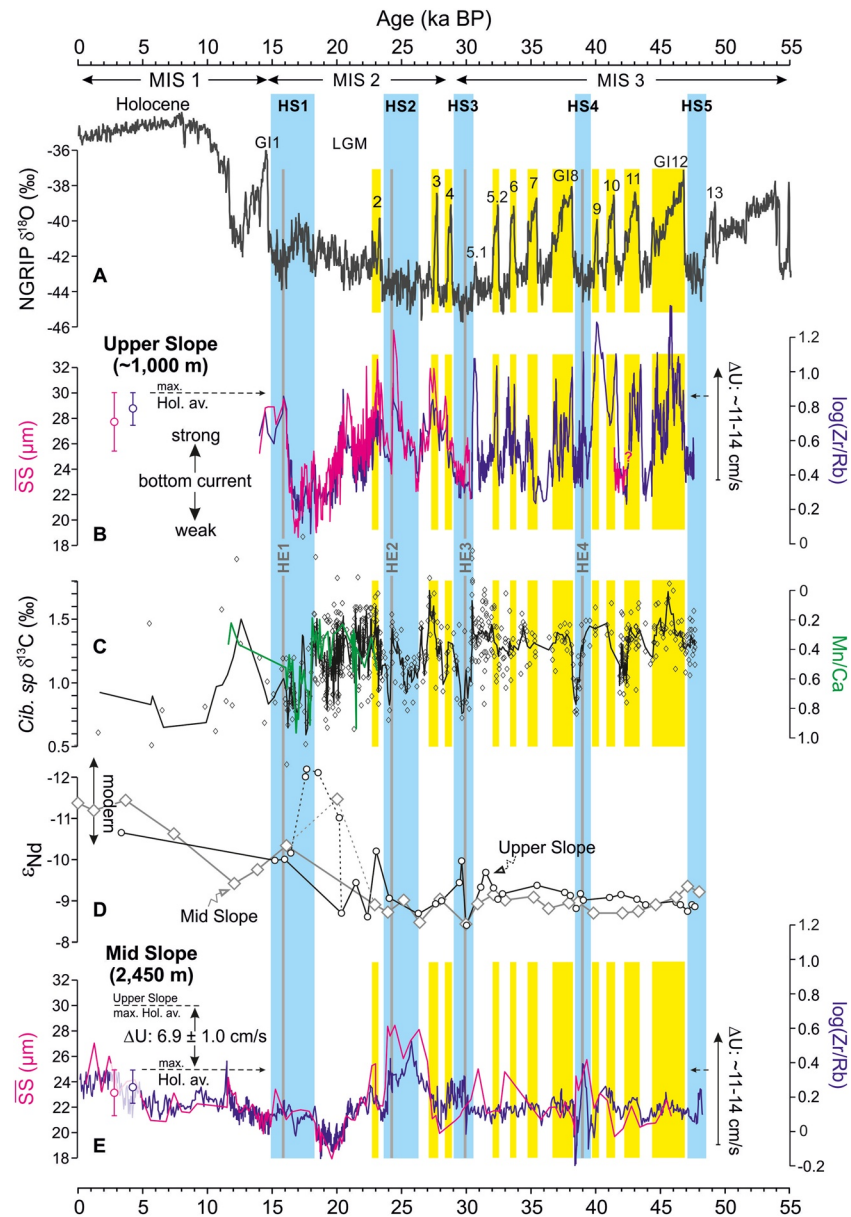### 5.1. Near-Bottom Flow Speed

The suitability of sediments of the upper (∼1,000 m water depth) and lower (2,450 m) French Atlantic slope to provide a reliable flow history was examined by testing the degree of correlation between the sortable silt mean size ($\overline{SS}$) and percentage (SS%) (McCave & Andrews, 2019; McCave, Manighetti, & Robinson, 1995). A positive relationship between $\overline{SS}$ and SS% is found for all the studied cores, with $\overline{SS}$—SS% correlation coefficients ranging from 0.69 (core BOB-CS03) to 0.91 (GIT-CS02), $\overline{SS}$—SS% slopes of 0.20 (MD04-2842)-0.47 (BOB-CS05) and intercepts at 5.8 (BOB-CS05)-16.2 μm (BOB-CS03) (Figure 2 and Table S3). These results, together with the comparison of Holocene $\overline{SS}$ (Table S4) with modern current meter data from the NE Atlantic (McCave et al., 2001; Pingree & Le Cann, 1989) and sedimentary evidence from downcore records (Stow & Holbrook, 1984), demonstrate that sorting processes at the studied sites are controlled by current flow dynamics (see Texts S1 and S2). Considering the requirements ("tests") of McCave and Andrews (2019), 75% of the $\overline{SS}$—SS% data set (794 of 1,055 samples) have a running downcore correlation (R$_{run}$; nine-point) >0.5 and a slope relationship >0.07 (Figure 2 and Figure S6). According to McCave & Andrews' (2019) recommendation, only these data were used for the paleocurrent reconstructions (Figures 4b and 4e).

$\overline{SS}$ and log (Zr/Rb) ratios show good correlations (0.65 < *r* < 0.85, *n* = 794) and are thus used together to investigate flow speed variability on the French Atlantic slope (Figure 3). However, we did not plot $\overline{SS}$ for the sandy (median grain size up to 150–200 μm), mixed clastic-biogenic MIS 3 contourites at ∼1,000 m depth, both because of the low proportions of the terrigenous sortable silt fraction (13.8 ± 9.3%, *n* = 150) and because the current-sorted biogenic component (∼30 wt.% minimum) is not captured by the (carbonate-free) $\overline{SS}$ proxy. In such a case, the use of the bulk log (Zr/Rb) ratio (including the detrital sand fraction), circumvents the problem of flow speed reconstructions from sandy, shell-rich contourites.

The mean $\overline{SS}$ and log (Zr/Rb) variabilities at ∼1,000 m are very consistent (in timing and magnitude) from one site to another (Figure S7). This indicates that each site from the upper slope records a common history of bottom current flow speed changes. Based on this evidence, we produce a composite record for $\overline{SS}$ and log (Zr/Rb) at ∼1,000 m (Figure 4b). The continuous, long-term log (Zr/Rb) records show significant differences between the upper and mid-slope over the last ∼50 kyr, with values ranging from ∼0.2 to 1.4 at ∼1,000 m water depth and reaching a maximum of only ∼0.6 at site MD04-2842, at 2,450 m (Figure 4e). This difference, revealing contourites of coarser texture on the upper slope, is corroborated by the $\overline{SS}$ data available at both sites for the Holocene (MIS 1; 27.8 ± 2.3 μm [*n* = 13] and 23.2 ± 1.8 μm [*n* = 16] at ∼1,000 m and 2,450 m, respectively; Table S4) and MIS 2 (25.1 ± 3.9 μm [*n* = 473] and 21.7 ± 2.3 μm [*n* = 65]). In addition, at long time scales, the average $\overline{SS}$ grain size (as well as the log (Zr/Rb) ratio) of glacial (>20 ka) conditions at ∼1,000 m (26.7 ± 3.5 μm [*n* = 298] for the 30–20 ka interval, with log (Zr/Rb) = 0.60 ± 0.30 [*n* = 3,146] for the 48–20 ka interval) is statistically indistinguishable from that of the Holocene (27.8 ± 2.3 μm [*n* = 13],

Figure 4. Reconstructions of ocean circulation changes on the French Atlantic margin over the last 50,000 years. (a) NGRIP $\delta^{18}O$ (GICC05 chronology; Rasmussen et al., 2006, 2014; Svensson et al., 2008). (b) Near-bottom flow speed (U) on the upper slope (∼1,000 m) reconstructed from $\overline{SS}$ (magenta line, three-point running average) and XRF log (Zr/Rb) (blue lines; three- and ten-point running average for the 30–0 and 48–30 ka intervals, respectively) composite records. Note that only the $\overline{SS}$(and associated XRF Zr/Rb) data "validated" by McCave & Andrews' (2019) recommendation are shown (see Section 5.1). The few "validated" data for the Holocene are shown through averages (see Table S4 for details). MIS 3 data are from core BOB-CS03. (c) Benthic $\delta^{13}C$ composite record from the upper slope (black line; three-point running average) and (benthic) foraminiferal Mn/Ca from core MD99-2328 (green line; Mojtahid et al., 2017). These data reflect the variability of bottom water ventilation (Figure S8). (d) Uncleaned foraminifera ε_{Nd} records from the upper ("stacked" data from BOB-CS03 and BOB-CS05; black line) and middepth cores (MD04-2842; gray line) (Table S6). The modern range of ε_{Nd} in the Bay of Biscay (0–3,000 m; Figure S9) is indicated (Copard et al., 2011; Dubois-Dauphin et al., 2017). Local inputs of European Ice Sheet sediment-laden meltwater likely explains the unradiogenic ε_{Nd} values at ∼20–17 ka (see Section 6.3 for details). (e) Near-bottom flow speed (U) on the middepth slope (2,450 m) reconstructed from $\overline{SS}$ (magenta line) and XRF Zr/Rb (blue line; three-point running average) data from core MD04-2842. Yellow bands: Greenland Interstadials (GI). Gray bands: Heinrich Events (HE). Light blue bands: Heinrich Stadials (HS). See Figures S3 and S4 for their definition in the local stratigraphic records. MIS: Marine Isotope Stage.

with log (Zr/Rb) = 0.76 ± 0.07 [n = 13]). On the other hand, $\overline{SS}$ at site MD04-2842 suggests slightly (though not statistically significant) higher values during the Holocene (23.2 ± 1.8 μm, n = 16) than during the last glacial period (21.8 ± 2.1 μm, n = 104). These data indicate more vigorous flow speed on the upper slope (∼1,000 m) while hinting at reduced bottom current strength on the mid-slope (2,450 m) during glacial conditions, over the last ∼50 kyr.

At the millennial time scale, bottom current flow speeds at ∼1,000 m are coupled to changes in Greenland climate as seen in the δ^{18}O ice record (Figures 4a and 4b). This is particularly evident for MIS 3 during which faster (slower) flow speeds are coeval with D-O interstadials (stadials) (Figure 4b and Figure S8). This relationship is also observed for MIS 2 (including HS2 and the LGM), but we note that during this period the flow speed variability remains as high as for MIS 3 (in amplitude and frequency) while the Greenland δ^{18}O variability tends to decrease (especially in amplitude). Finally, the flow speed minima at ∼1,000 m occurred at ∼19–16.5 ka [log (Zr/Rb) down to ∼0.1], a period encompassing the end of the LGM and the first part of HS1. The inferred flow speeds reconstructed for the preceding D-O and Heinrich stadials are systematically higher (Zr/Rb ∼0.3–0.4). The IRD-rich layers corresponding to HE4 (∼39 ka) and HE1 (∼16 ka) show high log (Zr/Rb) values on the upper slope (while low values characterized HE3 and HE2 at ∼30 ka and ∼24.2 ka, respectively). In the absence of $\overline{SS}$ data (sensitive to IRD if their concentration is >50%; McCave & Andrews, 2019), we cannot exclude the possibility that the Zr/Rb peak during HE4 reflects IRD inputs. On the other hand, the high $\overline{SS}$ [together with high log (Zr/Rb)] values observed during HE1 likely reflect high flow speed causing reduced fine deposition. This is supported first by the fact that high flow speed started before HE1 (as early as ∼16.5 ka) and persisted until ∼14.7 ka (Figure 4b), and second, by benthic foraminifera-based proxies showing concomitant well-oxygenated upper slope bottom waters (Mojtahid et al., 2017).

5.2. Bottom-Water Chemistry

Our benthic δ^{13}C data show a large variability of up to ∼0.8–1.0‰ on millennial timescales, with the lowest δ^{13}C values during HSs (∼0.6–0.8‰ at ∼1,000 m, and ∼0‰ at 2,450 m; Figure S2 and Table S5). The ice-volume corrected benthic δ^{18}O values (δ^{18}O$_{IVC}$; see Text S3) at ∼1,000 m show abrupt ∼0.5–1‰ decreases during the same intervals.

Our foraminiferal ε$_{Nd}$ records reveal core-top (i.e., upper Holocene) signatures of −10.6 ± 0.1 (n = 1) at ∼1,000 m and −11.3 ± 0.2 (n = 3) at 2,450 m (Figure 4d and Table S6). These ε$_{Nd}$ values are consistent with those of modern regional seawater and recent coral data from the French Atlantic margin (Copard et al., 2011; Dubois-Dauphin et al., 2017) as well as with foraminiferal data from the northern NE Atlantic (Crocker et al., 2016; Roberts & Piotrowski, 2015). Our results thus capture the modern regional water mass structure of the NE Atlantic with MOW overlying well-mixed NADW (Figure S9). Glacial (>20 ka) ε$_{Nd}$ values are more radiogenic at both depths (−9.1 ± 0.4 [n = 35] at ∼1,000 m, and −8.9 ± 0.2 [n = 20] at 2,450 m) (Figure 4d), revealing a different paleohydrographic structure for the glacial NE Atlantic.

6. Discussion

6.1. The French Atlantic Margin in the North Atlantic

Our data from the French Atlantic margin suggest little or no changes in average flow speed on the upper slope (∼1,000 m) at the glacial-interglacial timescale, consistent with NE Atlantic records at <2,000 m, for example around Rockall Bank (cores BOFS-11K, 14K and 17K; see Figure 9 in Manighetti & McCave, 1995) and on the South Iceland Rise (ODP Site 984; Moros et al., 1997; Praetorius et al., 2008). On the other hand, decreased average flow speeds are recorded in cores ≥2,500–4,000 m during the last glacial period on the Rockall region (Manighetti & McCave, 1995; McCave, Manighetti, & Beveridge, 1995) and the Iberian margin (Hall & McCave, 2000) and suggested at 2,450 m in the French Atlantic slope (this study). This suggests that glacial deep-water (≥2,500 m) circulation in the NE Atlantic was more sluggish than present while vigorous currents persisted at intermediate water depth. Similar results are obtained from depth transects and $\overline{SS}$ records in the western North Atlantic (Evans & Hall, 2008; Thornalley et al., 2013).

These sedimentological results agree with an active upper AMOC cell, although vertically contracted, persisting during the last glacial period as previously shown by various, independent geochemical proxies (i.e., benthic $\delta^{13}C$, ϵ_{Nd}, Cd/Ca, $^{231}Pa/^{230}Th$; Boyle & Keigwin, 1987; Curry & Oppo, 2005; Duplessy et al., 1988; Gherardi et al., 2009; Lippold et al., 2012; Marchitto & Broecker, 2006; Oppo & Lehman, 1993). This is also supported by our benthic $\delta^{13}C$ data that show better ventilated waters during the glacial than the Holocene above ~2,000 m whereas the opposite is observed below this depth (Figure S2), in agreement with studies from both the European margin (Crocker et al., 2016; Peck et al., 2006; Willamowski & Zahn, 2000; Zahn et al., 1997) and the western North Atlantic (Curry & Oppo, 2005; Keigwin, 2004; Lynch-Stieglitz et al., 2014; Zahn & Stüber, 2002).

The near-stability in the Holocene flow speed at ~1,000 m (standard deviation of 2.3 for $\overline{SS}$ and 0.07 for Zr/Rb) contrasts strikingly with the strong millennial-scale variability of glacial flow speeds (3.5 and 0.3, respectively). This glacial variability shows a remarkable stadial/slower-interstadial/faster pattern correlated to D-O variability, with flow speed changes >11–14 cm.s^{-1} according to the calibration relationships for $\overline{SS}$ of McCave et al. (2017) (Figure 4b). Most of these rapid changes, and in particular those related to the HSs, are associated with ~0.4 to ~0.8‰ shifts (negative during D-O and Heinrich stadials) in the benthic $\delta^{13}C$ values (Figure 4c). This glacial pattern for the benthic $\delta^{13}C$ strongly differs from that recorded at intermediate depths (<1,300 m) in the western North Atlantic (e.g., Caribbean Sea, Florida Straits, Bahamas; Boelaert, 1998; Curry et al., 1999; Lynch-Stieglitz et al., 2014; Willamowski & Zahn, 2000; Zahn & Stüber, 2002). In this region, the glacial benthic $\delta^{13}C$ records show similar first-order trends and average values (e.g., ~1.5‰ at the LGM) but HSs are not accompanied by any significant decrease in $\delta^{13}C$ (Figure S2). The $\delta^{13}C$ signature of HSs recognized on the upper French Atlantic slope is, however, widespread throughout the NE Atlantic as it has already been observed at similar depths (<1,600 m) on the Iberian margin (SO75-26-KL; Zahn et al., 1997), on the Porcupine Seabight (MD01-2461; Peck, Hall, Zahn, & Scourse, 2007) (Figure S2), in the southeastern Nordic Seas (Rasmussen & Thomsen, 2009), and on the South Iceland Rise (Praetorius et al., 2008; Willamowski & Zahn, 2000).

Despite some mismatches in amplitude and/or structure, the overall correspondence between our grain-size and benthic $\delta^{13}C$ data (Figure S8) suggests a correlation between near-bottom flow speed and water-mass ventilation at millennial timescales. Below, we show that the forcing of ocean current dynamics along the European margin can be differentiated from that of water mass chemical characteristics.

6.2. Mechanisms Driving Intermediate-Depth Circulation along the Western European Margin: The Glacial Eastern Boundary Current

6.2.1. Water Masses and Ocean Current Regime

Using multiple independent geochemical tracers of water mass properties (including foraminiferal ϵ_{Nd} values of -9.7 ± 1.1 on the ~45–20 ka interval) at ODP Site 980 (Rockall Bank), Crocker et al. (2016) have shown persistent ventilation of the glacial NE Atlantic down to ~2,200 m by NSW. The consistency of the ϵ_{Nd} signatures at ODP Site 980 with those recorded on the French Atlantic slope at ~1,000–2,450 m (-9.2 ± 0.5 on the same interval; $n = 46$), and the similarity of our carbon isotopic data (*C. wuellerstorfi*; $\delta^{13}C$ of ~1.2–1.6‰ at ~1,000 m and ~0.6‰ at 2,450 m; Figure S2) with the LGM distribution of benthic foraminiferal $\delta^{13}C$ in the North Atlantic (Curry & Oppo, 2005; Duplessy et al., 1988; Sarnthein et al., 1994), strengthen the hypothesis that the French Atlantic margin at intermediate depths was bathed by NSW during the last glacial period. This is consistent with previous results from the western European margin (Peck et al., 2006; Peck, Hall, Zahn, & Scourse, 2007; Zahn et al., 1997), and with the inability of the northward-flowing Antarctic Intermediate Water (AAIW) and MOW to explain our records. The AAIW did not reach latitudes north of southern Iberia during the last glacial period (Thornalley et al., 2015; Willamowski & Zahn, 2000) and the glacial MOW had a volume reduced by more than 50% (Rogerson et al., 2012; Zahn et al., 1997) with a stadial/faster-interstadial/slower variability opposite to that described here for the French Atlantic margin (Toucanne et al., 2007; Voelker et al., 2006). However, while NSW explain the benthic $\delta^{13}C$ and foraminiferal ϵ_{Nd} signatures found on the French Atlantic margin, the vigorous along-slope circulation imprinted in our $\overline{SS}$ and Zr/Rb records is more complex. Indeed, ocean dynamics (due to the

Earth's rotation) requires southward-flowing currents in the Northern Hemisphere (including the NSW) to be channeled toward the west (as is the DWBC today). Therefore, the NSW at the study sites has necessarily to be recirculated NSW transported eastward by the glacial NAC (GNAC) and ultimately entrained into the eastern boundary current (as today; Figure 1). Here we argue that the increases in near-bottom flow speeds recorded on the upper French Atlantic slope reflect the reinforcement of a northward-flowing Glacial Eastern Boundary Current (GEBC; Figure 5), that is a glacial version of the modern European Slope Current (Section 2; Figure 1).

6.2.2. Past Vigor of the GEBC: New Constraints on past AMOC Variability

The Northern Hemisphere ice-sheets strongly impacted North Atlantic atmospheric circulation during the last glacial period (Kageyama & Valdes, 2000; Pausata et al., 2011). At the LGM, the high and extensive LIS, located upwind of the ocean basin, forced the mid-latitude jet stream (Löfverström et al., 2014) and the GNAC to flow zonally and further south than at present (as far south as ∼40°N; Chapman & Shackleton, 1998; Keffer et al., 1988; Otto-Bliesner et al., 2006; Pflaumann et al., 2003). During MIS 3, the LIS was reduced in size relative to the LGM and numerical simulations suggest that the jet stream as well as the GNAC likely had a southwest-northeast oriented tilt (Löfverström et al., 2014). This pattern is supported by proxy and modeling evidence that suggest that the polar front in the glacial NE Atlantic, located directly north of the NAC (Krauss & Käse, 1984), was north of the British Isles during D-O interstadials (Li et al., 2010; Sadatzki et al., 2019; Scourse et al., 2009) (Figure 5a). However, southward shifts of the polar front toward mid-latitude Europe (as far south as the northern Iberian Peninsula) occurred during D-O stadials (Barker et al., 2015; Eynaud et al., 2009; Scourse et al., 2009), pointing out a LGM-like zonal flow of the GNAC during those time intervals (Figure 5b). This is supported by sedimentological evidence from the Azores Plateau showing strong winnowing of fine particles above ∼1,500 m water depth during cold intervals (Dennielou, 1997). These results taken together suggest strong latitudinal shifts in the position of the GNAC during MIS 3 (Chapman & Shackleton, 1998). Significant changes in the strength of the AMOC (Böhm et al., 2015; Henry et al., 2016; Waelbroeck et al., 2018), and hence of the North Atlantic SPG, accompanied these shifts (e.g., deeper, more vigorous overturning and stronger SPG during the D-O interstadials).

Recent observations suggest that the strength of the SPG (and, by extension, the NAC, which is the eastern limb of the SPG) controls the vigor of the European Slope Current (Marsh et al., 2017). By analogy with the modern period, we infer that the changes observed in the $\overline{SS}$ and Zr/Rb records on the French Atlantic margin may be related to basin-scale changes in the subpolar North Atlantic, including SPG variability and associated changes in meridional density gradients (see Section 2). We suggest that the weak flow speed on the upper slope during the D-O stadials originates from a weak GEBC (Figure 5b). An inflow of the (weak) GNAC into the Bay of Biscay cannot be excluded. Indeed, the zonal flow of the GNAC in the mid-Atlantic during stadials (according to reconstructions of the polar front) enables the GNAC to impinge south of the French Atlantic margin (Brady & Otto-Bliesner, 2011; Keffer et al., 1988). In either cases, the weak flow speed is indicative of a weak SPG (with corresponding shallow, weak overturning; Henry et al., 2016; Waelbroeck et al., 2018). On the other hand, during D-O interstadials, the GNAC had a southwest-northeast oriented tilt and impinged on the European margin north of the French Atlantic margin. Hence, the vigorous flow at the study site probably corresponded to a vigorous GEBC forced by a strong SPG during interstadials (Figure 5a). In simple terms, the interstadial/faster (stadial/slower) pattern of GEBC corresponds to enhanced (reduced) strength of the GNAC and, by extension, of enhanced (reduced) NSW production and AMOC during D-O interstadials (stadials). Our $\overline{SS}$ and Zr/Rb data provide the first record of millennial-scale changes in the strength of the northward AMOC flow, coherent with the changes in convection rates (Dokken & Jansen, 1999) and NSW export by the AMOC return flow in the western North Atlantic (Böhm et al., 2015; Henry et al., 2016) over the D-O events (Figures 6b and 6f).

6.3. Ice-Sheet—Ocean Interactions in the NE Atlantic and the AMOC Variability

Our results provide strong physical evidence that the strength of the AMOC varied during the studied stadial-interstadial oscillations (including the subdued GI-5.1), supporting the idea that glacial abrupt climate changes are associated with AMOC variability (Böhm et al., 2015; Gottschalk et al., 2015; Henry et al., 2016;
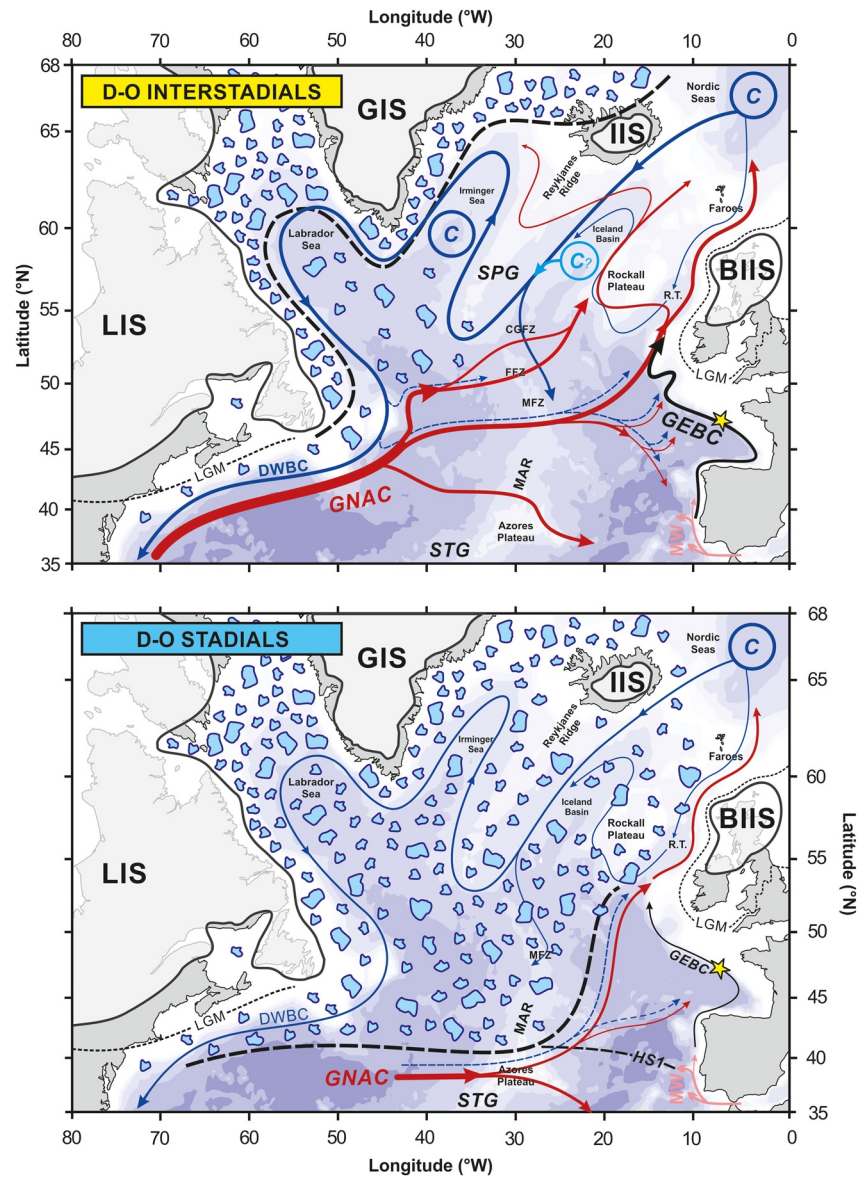
Figure 5. Schematic of the North Atlantic circulation during D-O interstadials (upper panel) and stadials (lower panel) of MIS 3. The red and blue continuous arrows indicate the NAC (as the main portion of the upper branch of the AMOC) and the southward return flow (lower branch) of AMOC, respectively. The Glacial Eastern Boundary Current (GEBC), that is a glacial version of the modern European Slope Current, is shown (black arrows). The black dashed lines show plausible scenarios for winter sea ice extent (15% ice concentration), equivalent to the polar front (Li et al., 2010). The strength of the GEBC is maximal during D-O interstadials. Our hypothesis is that this is due to enhanced production and export of intermediate-deep waters (NSW) in the northern North Atlantic open-ocean convection (C) sites (i.e., stronger strength of the subpolar gyre during D-O interstadials compared to D-O stadials). During D-O stadials, the GNAC would follow the polar front, precluding direct entrance of its main branch into the Bay of Biscay. During D-O interstadials and stadials, the GEBC is largely recruited from the eastern North Atlantic water masses (including recirculated NSW; dashed blue arrows). SPG: subpolar gyre. STG: subtropical gyre. BIIS: British-Irish Ice Sheet (that is the western part of the European Ice Sheet). IIS, Icelandic Ice Sheet; GIS, Greenland Ice Sheet; LIS, Laurentide Ice Sheet. The labels of the main topographical features are detailed in Figure 1. AMOC, Atlantic meridional overturning circulation; NAC, North Atlantic Current.
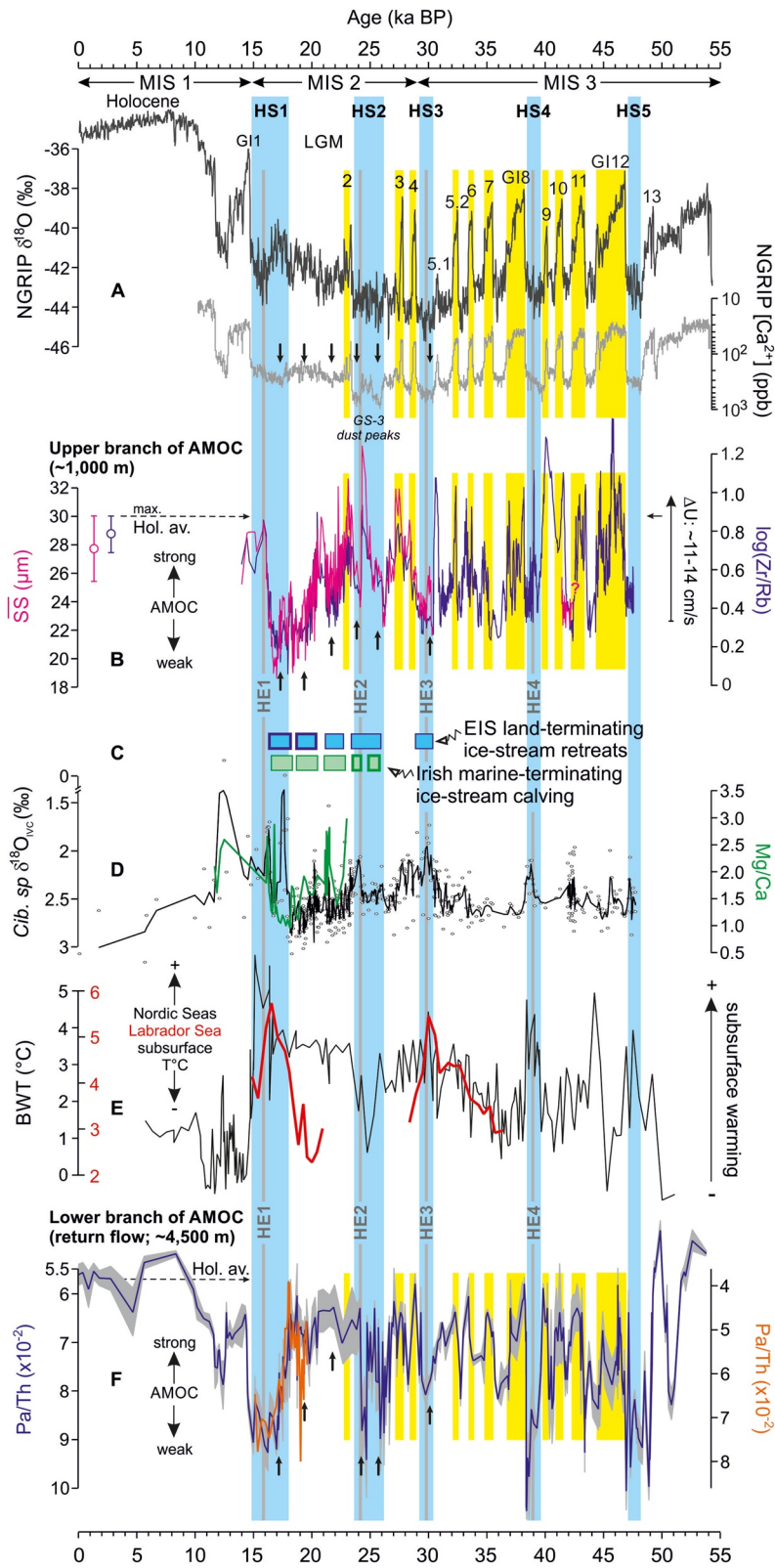
McManus et al., 2004; Waelbroeck et al., 2018). Our results also confirm that AMOC weakening (weak flow speeds) began well before the HEs (Henry et al., 2016; Zahn et al., 1997). This is robustly supported by our core stratigraphy (Figures 4b and 6b). Hence, if HEs may enhance and/or prolong cold stadial conditions through a positive feedback on the AMOC in response to the addition of freshwater, they were a consequence of these conditions rather than the cause (Barker et al., 2015; Bond & Lotti, 1995; Boswell et al., 2019; Clark et al., 2007). This agrees with data and modeling studies showing that HEs likely result from intermediate depth warming (Alvarez-Solas et al, 2010, 2013; Marcott et al., 2011; Shaffer et al., 2004), itself resulting from the AMOC weakening that no longer cools the interior of the low-latitude North Atlantic ocean sufficiently (Brady & Otto-Bliesner, 2011; Mignot et al., 2007; Shaffer et al., 2004). A detailed look at the European side of the North Atlantic may help to decipher the process determining the initial AMOC weakening.

Data and modeling studies suggest that ice-ocean interactions in the Nordic Seas could explain the D-O variability of MIS 3 (Alvarez-Solas et al., 2019; Dokken et al., 2013; Li et al., 2005, 2010; Rasmussen et al., 1996; Sadatzki et al., 2019; Wary et al., 2017). The European Ice Sheet (EIS), although restricted to Scandinavia during MIS 3 (Hughes et al., 2016), participated in these interactions through meltwater and calving (Brendryen et al., 2015; Lekens et al., 2006, 2009) with subsequent changes in buoyancy forcing and Nordic Seas convection strength (Dokken & Jansen, 1999). The significant changes in the strength of the GEBC, which was most likely fueling the Nordic Seas convection region as it does today, could reflect this variability in the ice-ocean interactions. The EIS grew rapidly after ∼35 ka (Hughes et al., 2016) and ice-ocean interactions extended southward (Peck, Hall, Zahn, Grousset, et al., 2007; Scourse et al., 2009) as far south as ∼50°N when the marine-terminating Irish Sea Ice Stream (ISIS) advanced into the Celtic Sea at ∼26 ka (Smedley, Scourse, et al., 2017). Although the southernmost limit of the Baltic Ice Stream in the northern European lowlands was reached up to 4,000 years later (∼22 ka), the presence of ice in the emerged North Sea allowed EIS meltwater from the continental interior of Europe (through a catchment of ∼2.5×10^6 km^2; Patton et al., 2017) to reach the NE Atlantic by ∼48°N from ∼30 ka to ∼17–16 ka (Toucanne et al., 2010, 2015). This ice sheet configuration, together with the pathway of both the GNAC and the GEBC (Figure 5), makes the western European margin an ideal location to explore the ice-sheet - ocean interactions during the second part of the last glacial period.

A striking example of ice-sheet—ocean interaction occurred during HS2, from ∼26 ka to 23.2 ka. This period is characterized in the North Atlantic region by two massive reorganizations of the atmospheric circulation at 26.0–25.1 ka and 24.2–23.4 ka (known as the "GS-3 dust peaks" in the Greenland ice; Rasmussen et al., 2014) separated by a warm SST event described along the western European margin (Austin et al., 2012; Waelbroeck et al., 2019). This short-lived event, recognized in our cores by a significant decrease in the *N. pachyderma* abundance (Figure S4), is coeval with a strong increase in the strength of the GEBC (Figure 6b). In the British Isles, the HS2 interval corresponds to a regional retreat of the marine ice streams offshore Ireland (Callard et al., 2018; O'Cofaigh et al., 2019), including the ISIS (Small et al., 2018; Smedley, Chiverrell, et al., 2017). This retreat occurred in two steps as shown by two discrete pulses in Irish-sourced IRD recorded on the western European margin (Knutz et al., 2007; Peck, Hall, Zahn, Grousset, et al., 2007; Scourse et al., 2000, 2009). Their identification on the French Atlantic slope (double IRD and *N. pachyderma* peaks at site MD95-2002; Grousset et al., 2000) reveals that these two episodes of ice retreat were synchronous with the two GEBC flow speed minima centered at ∼26–25 ka and ∼24–23.5 ka (Figures 6b and 6c). These decreases in GEBC intensity are coeval (within age uncertainties) with periods of severe

Figure 6. Ice-sheet—ocean interactions and the AMOC variability. (a) NGRIP δ^{18}O and [Ca^{2+}] (GICC05 chronology; Rasmussen et al., 2006, 2014; Svensson et al., 2008). (b) Near-bottom (∼1,000 m) GEBC flow speed changes reconstructed from the *SS* and Zr/Rb composite records. (c) Large-scale EIS fluctuations in the Baltic region (blue rectangles, core MD95-2002; Toucanne et al., 2015) and over the British Isles (green rectangles, core MD01-2461; Peck et al., 2006) associated to substantial freshwater inputs into the NE Atlantic. Rectangles with a thick border highlight the major events (see the main text for details). (d) "Stacked" ice-volume corrected benthic (*Cibicides* sp.) δ^{18}O (δ^{18}O$_{IVC}$) record (black line; three-point running average) for the upper French Atlantic margin (i.e., cores MD99-2328, CBT-CS10, BOB-CS03, GIT-CS02, and BOB-CS05, ∼1,000 m depth; see Text S3). Also shown is benthic Mg/Ca data from core MD99-2328 (green line; Mojtahid et al., 2017). (e) Mg/Ca-based bottom-water temperature (BWT) at ∼1,200 m from the Nordic Seas (JM11-FI-19PC; Ezat et al., 2014) and the Labrador Sea (EW9302-2JPC; Marcott et al., 2011). (f) Bermuda Rise ^{231}Pa/^{230}Th (blue line, with uncertainties in gray; Böhm et al., 2015; Henry et al., 2016) and Rockall Trough ^{231}Pa/^{230}Th (orange line; Hall et al., 2006) as a proxy for AMOC export. The vertical black arrows in (a), (b) and (f) refer to the large-scale EIS fluctuations summarized in (c). Yellow bands: Greenland Interstadials (GI). Light blue bands: Heinrich Stadials (HS). Gray bands: Heinrich Events (HE). See Figures S3 and S4 for their definition in the local stratigraphic records. MIS: Marine Isotope Stage. AMOC, Atlantic meridional overturning circulation; GEBC, Glacial Eastern Boundary Current.

weakening of NSW export in the deep western North Atlantic (Böhm et al., 2015; Gutjahr & Lippold, 2011) (Figure 6f). This correlation lends support to the idea that the calving episodes of the ISIS could have weakened the AMOC (Peck et al., 2006; Peck, Hall, Zahn, & Scourse, 2007). However, one could also argue that the destabilization of the ISIS during HS2 could result from intermediate depth warming, itself resulting from the AMOC weakening (e.g., Marcott et al., 2011). This subsurface warming is recorded along the European margin (southern Nordic Seas; Ezat et al., 2014) and suggested in our record as 0.3–0.5‰ decreases in $\delta^{18}O_{IVC}$ (Figures 6d and 6e). Notwithstanding this marine process, the ISIS retreat during HS2 is coeval with large meltwater inputs into the NE Atlantic (∼26–23 ka) in response to enhanced surface melting of land-terminating ice-streams of the EIS (western Baltic region; Boswell et al., 2019; Hughes et al., 2016; Toucanne et al., 2015). This continental process does not involve an oceanic-warming trigger, but importantly, requires summertime warming (Boswell et al., 2019). This atmospheric forcing could explain the onset of the ISIS retreat at ∼26–25 ka. If correct, freshwater inputs from both the western (ISIS) and southern (Baltic) margins of the EIS may explain the initial weakening of AMOC inferred from the reduced strength of the upper (GEBC, this study) and lower (Böhm et al., 2015) branches of the AMOC (Figures 6b and 6f). In turn, subsequent subsurface warming could have enhanced the ISIS retreat, while also triggering the HE2 signature recorded in our data at 24.2 ka (i.e., in the youngest flow speed minima; Alvarez-Solas et al., 2010; Marcott et al., 2011; Shaffer et al., 2004).

Like for HS2, the AMOC weakening episodes (suggested by both the GEBC records presented here and the deep western North Atlantic records of Böhm et al., 2015) at ∼30–29 ka (HS3), ∼22–21 ka, ∼20–19 ka and ∼18–17 ka (early HS1; Figures 6b and 6f) are coeval with periods of increased EIS melting (Figure 6c). This is shown by iceberg calving events west of the British Isles (Hall et al., 2011; Knutz et al., 2007; Peck et al., 2006; Scourse et al., 2009) and the concomitant retreat of the land-terminating ice-streams of the southern EIS that led to significant meltwater inputs to the NE Atlantic (Eynaud et al., 2012; Ménot et al., 2006; Toucanne et al., 2015; Zaragosi et al., 2001). The last two melting events are characterized by thick, fine-grained laminated deposits at the study site due to strong detrital inputs on the margin (Toucanne et al., 2010; Zaragosi et al., 2001). The preservation of millimetre-scale laminae, impossible under high-energy conditions, supports our interpretation for weak GEBC flow speed and AMOC. Concomitantly, it is likely that enhanced continental inputs would have influenced the Nd isotopic composition of the water column, through reversible scavenging and/or various sediment-seawater interactions (Jeandel & Oelkers, 2015; Siddall et al., 2008), thereby explaining the observed foraminiferal ε_{Nd} shifts toward unradiogenic values at those times (Figure 4d).

The tight link observed between EIS melting events (Figure 6c) and AMOC weakening (Figures 6b and 6f) between ∼30 and ∼17 ka emphasizes the role of the EIS on the negative buoyancy forcing in the northern North Atlantic. This is not surprising given that the meltwater releases discussed above occurred upstream of the main North Atlantic convection sites (Roche et al., 2010). This idea is reinforced by the fact that the EIS sediment-laden meltwaters, possibly evolving in the ocean as suspended load-dominated hyperpycnal flows traveling down the slope (Mulder et al., 2003), should have interacted with the poleward slope current (e.g. Miramontes et al., 2020). This would have promoted their direct advection to the Nordic Seas and reinforced their potential negative buoyancy forcing, leading to a subsequent decrease in AMOC strength.

6.4. Continuous Poleward Oceanic Heat Transport as a Driver for Glacial Climate Instability?

The ice-sheet—ocean interactions described along the western European margin during MIS 2, taken together with those described in the Nordic Seas during MIS 3 (Dokken et al., 2013; Rasmussen et al., 1996), identify the NE Atlantic as a key region for the generation of glacial abrupt climate changes. This is explained by the close proximity of the EIS to the convection sites (Roche et al., 2010), with the upper branch of the AMOC (i.e., GNAC and GEBC) providing the physical link between the two. On one hand, it "warms" the EIS by surface advection, triggering freshwater-forced perturbations (warm-to-cold transitions; e.g., Ganopolski & Rahmstorf, 2001). On the other, it carries warm intermediate waters (resulting from freshwater-forced AMOC weakening) to the subpolar North Atlantic, ultimately promoting AMOC reinvigoration (cold-to-warm transitions; e.g., Mignot et al., 2007). These warm waters are marked at our sites by 0.3–1‰ decreases in $\delta^{18}O_{IVC}$ and increased Mg/Ca ratio (Mojtahid et al., 2017, Figure 6d). It is worth noting that our data as well as those from the deep western North Atlantic suggest that a vigorous, although variable,

AMOC persisted until ∼19–18 ka, onset of the 3000- to 4000-year-long near-cessation of AMOC (Böhm et al., 2015; McManus et al., 2004; Ng et al., 2018). This leads us to hypothesize that a persistent glacial AMOC provides the necessary feedbacks, via oceanic heat transport at surface and intermediate depths, for the North Atlantic climate to switch back and forth between stadials (weak AMOC state) and interstadials (strong AMOC state). In simple terms, the AMOC is a self-limiting system whose most distinctive feature is the D-O variability of MIS 3 (see review of Menviel et al., 2020).

The variability in AMOC strength reported throughout the last glacial period, from intermediate- (MIS 3) to full-glacial conditions (MIS 2) (Figures 6b and 6f), raises questions about the near absence of D-O variability in ice core records from ∼28 ka to 15 ka (Figure 6a). We have shown that ice-sheet—ocean interactions operated down to the mid-latitudes during this interval. These interactions, involving subtle to significant changes in the AMOC strength and fluctuations of the polar front location, are interpreted here as being part of the millennial-scale variability observed during MIS 3. Their expression is, however, buffered by the high AMOC stability (i.e., less vulnerable ocean circulation) characterizing full glacial conditions (sea level ≤−80 m; Zhang & Prange, 2020). Only the ice-sheet—ocean interactions causing large freshwater anomalies in the North Atlantic significantly impact both the AMOC (e.g., Böhm et al., 2015) and the climate system (e.g., Barker et al., 2009), that is, during HS3, HS2, and HS1.

The intricacies of both ice-sheet—ocean interactions (including HEs) and AMOC changes registered in our marine cores during the HSs have no counterpart in the δ^{18}O of Greenland ice, including the complex structure of HS2 (Section 6.3) or HS1 in the NE Atlantic (Bard et al., 2000; Hodell et al., 2017; Toucanne et al., 2015; Zaragosi et al., 2001). This is consistent with the idea that Greenland δ^{18}O does not capture the full climatic variability of the North Atlantic region (Buizert, Keisling, et al., 2018; Landais et al., 2018). Our paleocurrent reconstruction reinforces this idea by showing a rapid, significant increase in GEBC strength in the second part of HS1, ∼16.5–14.7 ka, preceding by ∼1.5–2 kyr the resumption of AMOC in the deep western North Atlantic (>2,700 m; McManus et al., 2004; Ng et al., 2018). This reinforcement of the GEBC is coeval with increasing oxygenation on the French Atlantic slope (Mojtahid et al., 2017) and enhanced ventilation of middepth waters (<2,100 m) in the subtropical North Atlantic (Chen et al., 2015). Taken together, these results suggest an early reinvigoration in AMOC strength well before the Bølling warming but restricted to the upper ocean (≤2,000 m). This AMOC recovery, and the subsequent northward shift in the polar front in Europe (Cowling et al., 2020), likely explains the climate reorganization and hydroclimate shift observed in the North Atlantic region during HS1(Broecker & Putnam, 2012; Landais et al., 2018; Lincoln et al., 2020; Naughton et al., 2009). During this time, the upper branch of the AMOC also "pushed" northwards the subsurface warming (Figures 6d and 6e) initially caused by the preceding (∼18–16 ka) strong ice-sheet—ocean interactions (i.e., EIS melting and the HE1; Alvarez-Solas et al., 2011; Hodell et al., 2017; Ivanovic et al., 2018; Ng et al., 2018; Toucanne et al., 2015; Zaragosi et al., 2001). This could have contributed, by domino effect, to the AMOC overshoot (Barker et al., 2010; Liu et al., 2009) and the melting of the high-latitude, marine-based EIS involved in Meltwater Pulse 1A ∼14.65 ka (Brendryen et al., 2020). Further investigations are required to explore the role of this early reinvigoration of the AMOC in the last glacial termination.

7. Conclusions

We have reconstructed the strength of the northward-flowing GEBC in the North Atlantic, known today as the European Slope Current and representing the easternmost portion of the upper branch of the AMOC. Our high-resolution sedimentological proxies show that the GEBC strength at 1,000 m depth was highly variable through the ∼50–15 ka period and followed the D-O variability recognized in the North Atlantic region. Maximal (greater-than-Holocene) strength of the GEBC occurred during the D-O interstadials, while weakening of the GEBC occurred during the D-O and Heinrich stadials. This evolution of the kinematic proxies reflecting the upper branch of the AMOC is in overall good correspondence with the temporal changes of NSW export by the lower branch of AMOC seen in deep dynamic proxy records (e.g., Böhm et al., 2015; Henry et al., 2016; McManus et al., 2004).

The close proximity of the GEBC with the mid-latitude EIS during the latter part of the last glacial period allows us to explore ice-sheet—AMOC interactions in the NE Atlantic. We find that each EIS melting event,

marked by increased meltwater fluxes from both the marine- and land-terminating ice streams, was coeval with a decrease in the vigor of the GEBC and, more generally, of AMOC strength. These events, lying directly upstream of the convection sites, likely provided the buoyancy loss needed to decrease the formation and export of NSW. The major events (HSs) induced a significant subsurface warming due to large reductions in the AMOC that likely enhanced the melting of marine-based ice streams around the North Atlantic. This intermediate depth warming could have caused the collapse of the Hudson Strait ice stream (HEs) (Alvarez-Solas et al., 2010; Marcott et al., 2011). In this chain of events, the GEBC (together with the GNAC) transports northward both the EIS meltwater that causes the AMOC to weaken (warm-to-cold transition) and also the resulting intermediate depth warming that ultimately promotes AMOC reinvigoration (cold-to-warm transition). Since this reinvigoration favors ice-sheet mass loss and meltwater flux to the ocean (via surface heat advection), the interactions between the upper branch of the AMOC and the EIS lead the glacial North Atlantic climate to switch back and forth between stadials (weak AMOC state) and interstadials (strong AMOC state).

Our GEBC reconstruction is the first physical (non-chemical) record documenting dynamic upper AMOC variability at high resolution in the eastern basin of the North Atlantic. Together with the deep North Atlantic records of NSW export, they confirm the central role of the AMOC in the generation of abrupt climate changes.

Data Availability Statement

All data are available in SEANOE repository: https://doi.org/10.17882/77667

References

Alvarez-Solas, J., Banderas, R., Robinson, A., & Montoya, M. (2019). Ocean-driven millennial-scale variability of the Eurasian ice sheet during the last glacial period simulated with a hybrid ice-sheet-shelf model. *Climate of the Past*, *15*(3), 957–979. https://doi.org/10.5194/cp-15-957-2019

Alvarez-Solas, J., Charbit, S., Ritz, C., Paillard, D., Ramstein, G., & Dumas, C. (2010). Links between ocean temperature and iceberg discharge during Heinrich events. *Nature Geoscience*, *3*(2), 122–126. https://doi.org/10.1038/ngeo752

Álvarez-Solas, J., Montoya, M., Ritz, C., Ramstein, G., Charbit, S., Dumas, C., et al. (2011). Heinrich event 1: An example of dynamical ice-sheet reaction to oceanic changes. *Climate of the Past*, *7*(4), 1297–1306. https://doi.org/10.5194/cp-7-1297-2011

Alvarez-Solas, J., Robinson, A., Montoya, M., & Ritz, C. (2013). Iceberg discharges of the last glacial period driven by oceanic circulation changes. *Proceedings of the National Academy of Sciences*, *110*(41), 16350–16354. https://doi.org/10.1073/pnas.1306622110

Arzel, O., Colin de Verdière, A., & England, M. H. (2010). The role of oceanic heat transport and wind stress forcing in abrupt millennial-scale climate transitions. *Journal of Climate*, *23*(9), 2233–2256. https://doi.org/10.1175/2009jcli3227.1

Austin, W. E. N., Hibbert, F. D., Rasmussen, S. O., Peters, C., Abbott, P. M., & Bryant, C. L. (2012). The synchronization of paleoclimatic events in the North Atlantic region during Greenland Stadial 3 (ca 27.5 to 23.3kyr b2k). *Quaternary Science Reviews*, *36*, 154–163. https://doi.org/10.1016/j.quascirev.2010.12.014

Bard, E., Rostek, F., Turon, J.-L., & Gendreau, S. (2000). Hydrological impact of Heinrich events in the subtropical northeast Atlantic. *Science*, *289*(5483), 1321–1324. https://doi.org/10.1126/science.289.5483.1321

Barker, S., Chen, J., Gong, X., Jonkers, L., Knorr, G., & Thornalley, D. (2015). Icebergs not the trigger for North Atlantic cold events. *Nature*, *520*(7547), 333–336. https://doi.org/10.1038/nature14330

Barker, S., Diz, P., Vautravers, M. J., Pike, J., Knorr, G., Hall, I. R., & Broecker, W. S. (2009). Interhemispheric Atlantic seesaw response during the last deglaciation. *Nature*, *457*(7233), 1097–1102. https://doi.org/10.1038/nature07770

Barker, S., Knorr, G., Vautravers, M. J., Diz, P., & Skinner, L. C. (2010). Extreme deepening of the Atlantic overturning circulation during deglaciation. *Nature Geoscience*, *3*(8), 567–571. https://doi.org/10.1038/ngeo921

Berx, B., Hansen, B., Østerhus, S., Larsen, K. M., Sherwin, T., & Jochumsen, K. (2013). Combining in-situ measurements and altimetry to estimate volume, heat and salt transport variability through the Faroe Shetland Channel. *Ocean Science Discussions*, *10*(1).

Blaauw, M. (2010). Methods and code for 'classical' age-modeling of radiocarbon sequences. *Quaternary Geochronology*, *5*(5), 512–518. https://doi.org/10.1016/j.quageo.2010.01.002

Boelaert, A. (1998). *Variabilité de la circulation de surface et intermédiaire aux moyennes latitudes de l'Atlantique nord: Réponse aux variations lentes et rapides du climat lors du dernier cycle glaciaire - interglaciaire* (Unpublished PhD thesis). Brest: Université de Bretagne Occidentale.

Boers, N., Ghil, M., & Rousseau, D.-D. (2018). Ocean circulation, ice shelf, and sea ice interactions explain Dansgaard-Oeschger cycles. *Proceedings of the National Academy of Sciences of the United States of America*, *115*(47), E11005–E11014. https://doi.org/10.1073/pnas.1802573115

Böhm, E., Lippold, J., Gutjahr, M., Frank, M., Blaser, P., Antz, B., et al. (2015). Strong and deep Atlantic meridional overturning circulation during the last glacial cycle. *Nature*, *517*(7532), 73–76. https://doi.org/10.1038/nature14059

Bond, G. C., & Lotti, R. (1995). Iceberg discharges into the North Atlantic on millennial time scales during the last glaciation. *Science*, *267*(5200), 1005–1010. https://doi.org/10.1126/science.267.5200.1005

Booth, D. A., & Ellett, D. J. (1983). The Scottish continental slope current. *Continental Shelf Research*, *2*(2–3), 127–146. https://doi.org/10.1016/0278-4343(83)90012-2

Boswell, S. M., Toucanne, S., Pitel-Roudaut, M., Creyts, T. T., Eynaud, F., & Bayon, G. (2019). Enhanced surface melting of the Fennoscandian Ice Sheet during periods of North Atlantic cooling. *Geology*, *47*(7), 664–668. https://doi.org/10.1130/g46370.1

Bouvier, A., Vervoort, J. D., & Patchett, P. J. (2008). The Lu-Hf and Sm-Nd isotopic composition of CHUR: Constraints from unequilibrated chondrites and implications for the bulk composition of terrestrial planets. *Earth and Planetary Science Letters*, *273*(1–2), 48–57. https://doi.org/10.1016/j.epsl.2008.06.010

Bower, A. S., Lozier, M. S., Gary, S. F., & Böning, C. W. (2009). Interior pathways of the North Atlantic meridional overturning circulation. *Nature*, *459*(7244), 243–247. https://doi.org/10.1038/nature07979

Boyle, E. A., & Keigwin, L. (1987). North Atlantic thermohaline circulation during the past 20,000 years linked to high-latitude surface temperature. *Nature*, *330*(6143), 35–40. https://doi.org/10.1038/330035a0

Brady, E. C., & Otto-Bliesner, B. L. (2011). The role of meltwater-induced subsurface ocean warming in regulating the Atlantic meridional overturning in glacial climate simulations. *Climate Dynamics*, *37*(7–8), 1517–1532. https://doi.org/10.1007/s00382-010-0925-9

Brendryen, J., Haflidason, H., Rise, L., Chand, S., Vanneste, M., Longva, O., et al. (2015). Ice sheet dynamics on the Lofoten-Vesterålen shelf, north Norway, from Late MIS-3 to Heinrich Stadial 1. *Quaternary Science Reviews*, *119*, 136–156. https://doi.org/10.1016/j.quascirev.2015.03.015

Brendryen, J., Haflidason, H., Yokoyama, Y., Haaga, K. A., & Hannisdal, B. (2020). Eurasian ice sheet collapse was a major source of meltwater pulse 1A 14,600 years ago. *Nature Geoscience*, *13*(5), 363–368. https://doi.org/10.1038/s41561-020-0567-4

Broecker, W., & Putnam, A. E. (2012). How did the hydrologic cycle respond to the two-phase mystery interval? *Quaternary Science Reviews*, *57*, 17–25. https://doi.org/10.1016/j.quascirev.2012.09.024

Broecker, W. S. (1991). The great ocean conveyor. *Oceanography*, *4*(2), 79–89.

Broecker, W. S., Bond, G., Klas, M., Bonani, G., & Wolfli, W. (1990). A salt oscillator in the glacial Atlantic? 1. The concept. *Paleoceanography*, *5*(4), 469–477. https://doi.org/10.1029/pa005i004p00469

Broecker, W. S., & Denton, G. H. (1990). The role of ocean-atmosphere reorganizations in glacial cycles. *Quaternary Science Reviews*, *9*(4), 305–341. https://doi.org/10.1016/0277-3791(90)90026-7

Buckley, M. W., & Marshall, J. (2016). Observations, inferences, and mechanisms of the Atlantic meridional overturning circulation: A review. *Reviews of Geophysics*, *54*(1), 5–63. https://doi.org/10.1002/2015rg000493

Buizert, C., Keisling, B. A., Box, J. E., He, F., Carlson, A. E., Sinclair, G., & DeConto, R. M. (2018). Greenland-wide seasonal temperatures during the last deglaciation. *Geophysical Research Letters*, *45*(4), 1905–1914. https://doi.org/10.1002/2017gl075601

Buizert, C., Sigl, M., Severi, M., Markle, B. R., Wettstein, J. J., McConnell, J. R., et al. (2018). Abrupt ice-age shifts in southern westerly winds and Antarctic climate forced from the north. *Nature*, *563*(7733), 681–685. https://doi.org/10.1038/s41586-018-0727-5

Callard, S. L., Cofaigh, C. Ó., Benetti, S., Chiverrell, R. C., Van Landeghem, K. J. J., Saher, M. H., et al. (2018). Extent and retreat history of the Barra Fan Ice Stream offshore western Scotland and Northern Ireland during the last glaciation. *Quaternary Science Reviews*, *201*, 280–302. https://doi.org/10.1016/j.quascirev.2018.10.002

Chapman, M. R., & Shackleton, N. J. (1998). Millennial-scale fluctuations in North Atlantic heat flux during the last 150,000 years. *Earth and Planetary Science Letters*, *159*(1–2), 57–70. https://doi.org/10.1016/s0012-821x(98)00068-5

Chen, J., Chen, Y., Liu, L., Ji, J., Balsam, W., Sun, Y., & Lu, H. (2006). Zr/Rb ratio in the Chinese loess sequences and its implication for changes in the East Asian winter monsoon strength. *Geochimica et Cosmochimica Acta*, *70*(6), 1471–1482. https://doi.org/10.1016/j.gca.2005.11.029

Chen, T., Robinson, L. F., Burke, A., Southon, J., Spooner, P., Morris, P. J., & Ng, H. C. (2015). Synchronous centennial abrupt events in the ocean and atmosphere during the last deglaciation. *Science*, *349*(6255), 1537–1541. https://doi.org/10.1126/science.aac6159

Clark, P. U., S. W. Hostetler, N. G. Pisias, A. Schmittner, and K. J. Meissner (2007). Mechanisms for an ∼7-kyr climate and sea-level oscillation during marine isotope stage 3. In A. Schmittner et al. (Ed.) *Ocean Circulation: Mechanisms and Impacts, Geophysical Monograph Series* (Vol. 173, p. 209–246). AGU, Washington, D. C.

Copard, K., Colin, C., Frank, N., Jeandel, C., Montero-Serrano, J.-C., Reverdin, G., & Ferron, B. (2011). Nd isotopic composition of water masses and dilution of the Mediterranean outflow along the southwest European margin. *Geochemistry, Geophysics, Geosystems*, *12*(6). https://doi.org/10.1029/2011gc003529

Cowling, O. C., Thomas, E. K., Svendsen, J. I., Mangerud, J., Vasskog, K., & Haflidason, H. (2020). Northward shifts in the polar front preceded Bølling and Holocene warming in southwestern Scandinavia. *Geophysical Research Letters*, *47*(14), e2020GL088153. https://doi.org/10.1029/2020gl088153

Crocker, A. J., Chalk, T. B., Bailey, I., Spencer, M. R., Gutjahr, M., Foster, G. L., & Wilson, P. A. (2016). Geochemical response of the mid-depth Northeast Atlantic Ocean to freshwater input during Heinrich events 1 to 4. *Quaternary Science Reviews*, *151*, 236–254. https://doi.org/10.1016/j.quascirev.2016.08.035

Curry, W. B., Marchitto, T. M., McManus, J. F., Oppo, D. W., & Laarkamp, K. L. (1999). Millennial-scale changes in ventilation of the thermocline, intermediate, and deep waters of the glacial North Atlantic. *Geophysical Monograph-American Geophysical Union*, *112*, 59–76. https://doi.org/10.1029/gm112p0059

Curry, W. B., & Oppo, D. W. (2005). Glacial water mass geometry and the distribution of δ13C of ΣCO2 in the western Atlantic Ocean. *Paleoceanography*, *20*(1). https://doi.org/10.1029/2004pa001021

Daniault, N., Mercier, H., Lherminier, P., Sarafanov, A., Falina, A., Zunino, P., et al. (2016). The northern North Atlantic Ocean mean circulation in the early 21st century. *Progress in Oceanography*, *146*, 142–158. https://doi.org/10.1016/j.pocean.2016.06.007

Dansgaard, W., Johnsen, S. J., Clausen, H. B., Dahl-Jensen, D., Gundestrup, N. S., Hammer, C. U., et al. (1993). Evidence for general instability of past climate from a 250-kyr ice-core record. *Nature*, *364*(6434), 218–220. https://doi.org/10.1038/364218a0

de Madron, X. D., Castaing, P., Nyffeler, F., & Courp, T. (1999) Slope transport of suspended particulate matter on the Aquitanian margin of the Bay of Biscay. *Deep Sea Research Part II: Topical Studies in Oceanography*, *46*(10), 2003–2027.

Dennielou, B. (1997). *Sedimentary dynamic on the Azores plateau during the last 400 ka: Distribution, lithology, fluxes and processes* (PhD thesis). Brest: Université de Bretagne Occidentale. https://archimer.ifremer.fr/doc/00034/14505/

Dickson, R. R., & Brown, J. (1994). The production of North Atlantic Deep Water: sources, rates, and pathways. *Journal of Geophysical Research*, *99*(C6), 12319–12341. https://doi.org/10.1029/94jc00530

Dokken, T. M., & Jansen, E. (1999). Rapid changes in the mechanism of ocean convection during the last glacial period. *Nature*, *401*(6752), 458–461. https://doi.org/10.1038/46753

Dokken, T. M., Nisancioglu, K. H., Li, C., Battisti, D. S., & Kissel, C. (2013). Dansgaard-Oeschger cycles: Interactions between ocean and sea ice intrinsic to the Nordic seas. *Paleoceanography*, *28*(3), 491–502. https://doi.org/10.1002/palo.20042

Du, J., Haley, B. A., & Mix, A. C. (2020). Evolution of the Global Overturning Circulation since the Last Glacial Maximum based on marine authigenic neodymium isotopes. *Quaternary Science Reviews*, *241*, 106396. https://doi.org/10.1016/j.quascirev.2020.106396

Dubois-Dauphin, Q., Colin, C., Bonneau, L., Montagna, P., Wu, Q., Van Rooij, D., et al. (2017). Fingerprinting Northeast Atlantic water masses using neodymium isotopes. *Geochimica et Cosmochimica Acta*, *210*, 267–288. https://doi.org/10.1016/j.gca.2017.04.002

Duplessy, J. C., Shackleton, N. J., Fairbanks, R. G., Labeyrie, L., Oppo, D., & Kallel, N. (1988). Deepwater source variations during the last climatic cycle and their impact on the global deepwater circulation. *Paleoceanography*, *3*(3), 343–360. https://doi.org/10.1029/pa003i003p00343

Dypvik, H., & Harris, N. B. (2001). Geochemical facies analysis of fine-grained siliciclastics using Th/U, Zr/Rb and (Zr+Rb)/Sr ratios. *Chemical Geology*, *181*(1–4), 131–146. https://doi.org/10.1016/s0009-2541(01)00278-9

Eide, M., Olsen, A., Ninnemann, U. S., & Johannessen, T. (2017). A global ocean climatology of preindustrial and modern ocean $\delta^{13}C$. *Global Biogeochemical Cycles*, *31*(3), 515–534. https://doi.org/10.1002/2016gb005473

Elliot, M., Labeyrie, L., & Duplessy, J.-C. (2002). Changes in North Atlantic deep-water formation associated with the Dansgaard-Oeschger temperature oscillations (60-10ka). *Quaternary Science Reviews*, *21*(10), 1153–1165. https://doi.org/10.1016/s0277-3791(01)00137-8

EPICA Community Members (2006). One-to-one coupling of glacial climate variability in Greenland and Antarctica. *Nature*, *444*(7116), 195.

Evans, H. K., & Hall, I. R. (2008). Deepwater circulation on Blake Outer Ridge (western North Atlantic) during the holocene, younger dryas, and last glacial maximum. *Geochemistry, Geophysics, Geosystems*, *9*(3). https://doi.org/10.1029/2007gc001771

Eynaud, F., De Abreu, L., Voelker, A., Schönfeld, J., Salgueiro, E., Turon, J.-L., et al. (2009). Position of the Polar Front along the western Iberian margin during key cold episodes of the last 45 ka. *Geochemistry, Geophysics, Geosystems*, *10*(7). https://doi.org/10.1029/2009gc002398

Eynaud, F., Malaizé, B., Zaragosi, S., De Vernal, A., Scourse, J., Pujol, C., et al. (2012). New constraints on European glacial freshwater releases to the North Atlantic Ocean. *Geophysical Research Letters*, *39*(15). https://doi.org/10.1029/2012gl052100

Ezat, M. M., Rasmussen, T. L., & Groeneveld, J. (2014). Persistent intermediate water warming during cold stadials in the southeastern Nordic seas during the past 65 k.y. *Geology*, *42*(8), 663–666. https://doi.org/10.1130/g35579.1

Friocourt, Y., Drijfhout, S., & Blanke, B. (2008). On the dynamics of the slope current system along the West European Margin. Part I: Analytical calculations and numerical simulations with steady-state forcing. *Journal of Physical Oceanography*, *38*(12), 2597–2618. https://doi.org/10.1175/2008jpo3744.1

Friocourt, Y., Levier, B., Speich, S., Blanke, B., & Drijfhout, S. S. (2007). A regional numerical ocean model of the circulation in the Bay of Biscay. *Journal of Geophysical Research: Oceans*, *112*(C9). https://doi.org/10.1029/2006jc003935

Ganopolski, A., & Rahmstorf, S. (2001). Rapid changes of glacial climate simulated in a coupled climate model. *Nature*, *409*(6817), 153–158. https://doi.org/10.1038/35051500

Ganopolski, A., Rahmstorf, S., Petoukhov, V., & Claussen, M. (1998). Simulation of modern and glacial climates with a coupled global model of intermediate complexity. *Nature*, *391*(6665), 351–356. https://doi.org/10.1038/34839

Gherardi, J.-M., Labeyrie, L., Nave, S., Francois, R., McManus, J. F., & Cortijo, E. (2009). Glacial-interglacial circulation changes inferred from $^{231}Pa/^{230}Th$ sedimentary record in the North Atlantic region. *Paleoceanography*, *24*(2). https://doi.org/10.1029/2008pa001696

Gildor, H., & Tziperman, E. (2003). Sea-ice switches and abrupt climate change. *Philosophical Transactions of the Royal Society of London, Series A: Mathematical, Physical and Engineering Sciences*, *361*(1810), 1935–1944. https://doi.org/10.1098/rsta.2003.1244

Gottschalk, J., Skinner, L. C., Misra, S., Waelbroeck, C., Menviel, L., & Timmermann, A. (2015). Abrupt changes in the southern extent of North Atlantic Deep Water during Dansgaard-Oeschger events. *Nature Geoscience*, *8*(12), 950–954. https://doi.org/10.1038/ngeo2558

Grousset, F. E., Pujol, C., Labeyrie, L., Auffret, G., & Boelaert, A. (2000). Were the North Atlantic Heinrich events triggered by the behavior of the European ice sheets? *Geology*, *28*(2), 123–126. https://doi.org/10.1130/0091-7613(2000)028<0123:wtnahe>2.3.co;2

Gutjahr, M., & Lippold, J. (2011). Early arrival of Southern Source Water in the deep North Atlantic prior to Heinrich event 2. *Paleoceanography*, *26*(2). https://doi.org/10.1029/2011pa002114

Hall, I. R., Colmenero-Hidalgo, E., Zahn, R., Peck, V. L., & Hemming, S. R. (2011). Centennial-to millennial-scale ice-ocean interactions in the subpolar northeast Atlantic 18–41 kyr ago. *Paleoceanography*, *26*(2). https://doi.org/10.1029/2010pa002084

Hall, I. R., & McCave, I. N. (2000). Palaeocurrent reconstruction, sediment and thorium focusing on the Iberian margin over the last 140 ka. *Earth and Planetary Science Letters*, *178*(1–2), 151–164. https://doi.org/10.1016/s0012-821x(00)00068-6

Hall, I. R., Moran, S. B., Zahn, R., Knutz, P. C., Shen, C.-C., & Edwards, R. L. (2006). Accelerated drawdown of meridional overturning in the late-glacial Atlantic triggered by transient pre-H event freshwater perturbation. *Geophysical Research Letters*, *33*(16). https://doi.org/10.1029/2006gl026239

Hall, M. M., & Bryden, H. L. (1982). Direct estimates and mechanisms of ocean heat transport. *Deep Sea Research Part A. Oceanographic Research Papers*, *29*(3), 339–359. https://doi.org/10.1016/0198-0149(82)90099-1

Hemming, S. R. (2004). Heinrich events: Massive late Pleistocene detritus layers of the North Atlantic and their global climate imprint. *Reviews of Geophysics*, *42*(1). https://doi.org/10.1029/2003rg000128

Henry, L. G., McManus, J. F., Curry, W. B., Roberts, N. L., Piotrowski, A. M., & Keigwin, L. D. (2016). North Atlantic Ocean circulation and abrupt climate change during the last glaciation. *Science*, *353*(6298), 470–474. https://doi.org/10.1126/science.aaf5529

Hernández-Molina, F. J., Serra, N., Stow, D. A. V., Llave, E., Ercilla, G., & Van Rooij, D. (2011). Along-slope oceanographic processes and sedimentary products around the Iberian margin. *Geo-Marine Letters*, *31*(5–6), 315–341. https://doi.org/10.1007/s00367-011-0242-2

Hodell, D. A., Nicholl, J. A., Bontognali, T. R. R., Danino, S., Dorador, J., Dowdeswell, J. A., et al. (2017). Anatomy of Heinrich Layer 1 and its role in the last deglaciation. *Paleoceanography*, *32*(3), 284–303. https://doi.org/10.1002/2016pa003028

Hoogakker, B. A. A., Downy, F., Andersson, M. A., Chapman, M. R., Elderfield, H., McCave, I. N., et al. (2013). Gulf Stream—Subtropical gyre properties across two Dansgaard-Oeschger cycles. *Quaternary Science Reviews*, *81*, 105–113. https://doi.org/10.1016/j.quascirev.2013.09.020

Hoogakker, B., McCave, I., & Vautravers, M. (2007). Antarctic link to deep flow speed variation during Marine Isotope Stage 3 in the western North Atlantic. *Earth and Planetary Science Letters*, *257*(3–4), 463–473. https://doi.org/10.1016/j.epsl.2007.03.003

Houpert, L., Cunningham, S., Fraser, N., Johnson, C., Holliday, N. P., Jones, S., et al. (2020). Observed variability of the North Atlantic Current in the Rockall trough from 4 years of mooring measurements. *Journal of Geophysical Research: Oceans*, *125*(10), e2020JC016403. https://doi.org/10.1029/2020jc016403

Houpert, L., Inall, M. E., Dumont, E., Gary, S., Johnson, C., Porter, M., et al. (2018). Structure and transport of the North Atlantic Current in the eastern subpolar gyre from sustained glider observations. *Journal of Geophysical Research: Oceans*, *123*(8), 6019–6038. https://doi.org/10.1029/2018jc014162

Hughes, A. L. C., Gyllencreutz, R., Lohne, Ø. S., Mangerud, J., & Svendsen, J. I. (2016). The last Eurasian ice sheets—A chronological database and time-slice reconstruction, DATED-1. *Boreas*, *45*(1), 1–45. https://doi.org/10.1111/bor.12142

Huthnance, J. M. (1984). Slope Currents and "JEBAR". *Journal of Physical Oceanography*, *14*(4), 795–810. https://doi.org/10.1175/1520-0485(1984)014<0795:sca>2.0.co;2

Huthnance, J. M. (1986). The Rockall slope current and shelf-edge processes. *Proceedings of the Royal Society of Edinburgh. Section B: Biological Sciences*, *88*, 83–101. https://doi.org/10.1017/s0269727000004486

Huthnance, J. M., Inall, M. E., & Fraser, N. J. (2020). Oceanic density/pressure gradients and slope currents. *Journal of Physical Oceanography*, *50*(6), 1643–1654. https://doi.org/10.1175/jpo-d-19-0134.1

Iorga, M. C., & Lozier, M. S. (1999). Signatures of the Mediterranean outflow from a North Atlantic climatology: 1. Salinity and density fields. *Journal of Geophysical Research*, *104*(C11), 25985–26009. https://doi.org/10.1029/1999jc900115

Ivanovic, R. F., Gregoire, L. J., Burke, A., Wickert, A. D., Valdes, P. J., Ng, H. C., et al. (2018). Acceleration of northern ice sheet melt induces AMOC slowdown and northern cooling in simulations of the early last deglaciation. *Paleoceanography and Paleoclimatology*, *33*(7), 807–824. https://doi.org/10.1029/2017pa003308

Jeandel, C., & Oelkers, E. H. (2015). The influence of terrigenous particulate material dissolution on ocean chemistry and global element cycles. *Chemical Geology*, *395*, 50–66. https://doi.org/10.1016/j.chemgeo.2014.12.001

Kageyama, M., & Valdes, P. J. (2000). Impact of the North American ice-sheet orography on the Last Glacial Maximum eddies and snowfall. *Geophysical Research Letters*, *27*(10), 1515–1518. https://doi.org/10.1029/1999gl011274

Keffer, T., Martinson, D. G., & Corliss, B. H. (1988). The position of the Gulf Stream during Quaternary glaciations. *Science*, *241*(4864), 440–442. https://doi.org/10.1126/science.241.4864.440

Keigwin, L. D. (2004). Radiocarbon and stable isotope constraints on Last Glacial Maximum and Younger Dryas ventilation in the western North Atlantic. *Paleoceanography*, *19*(4). https://doi.org/10.1029/2004pa001029

Keigwin, L. D., & Jones, G. A. (1994). Western North Atlantic evidence for millennial-scale changes in ocean circulation and climate. *Journal of Geophysical Research*, *99*(C6), 12397–12410. https://doi.org/10.1029/94jc00525

Kissel, C., Laj, C., Piotrowski, A. M., Goldstein, S. L., & Hemming, S. R. (2008). Millennial-scale propagation of Atlantic deep waters to the glacial Southern Ocean. *Paleoceanography*, *23*(2). https://doi.org/10.1029/2008pa001624

Knutz, P. C., Zahn, R., & Hall, I. R. (2007). Centennial-scale variability of the British Ice Sheet: Implications for climate forcing and Atlantic meridional overturning circulation during the last deglaciation. *Paleoceanography*, *22*(1). https://doi.org/10.1029/2006pa001298

Krauss, W., & Käse, R. H. (1984). Mean circulation and eddy kinetic energy in the eastern North Atlantic. *Journal of Geophysical Research*, *89*(C3), 3407–3415. https://doi.org/10.1029/jc089ic03p03407

Kylander, M. E., Ampel, L., Wohlfarth, B., & Veres, D. (2011). High-resolution X-ray fluorescence core scanning analysis of Les Echets (France) sedimentary sequence: new insights from chemical proxies. *Journal of Quaternary Science*, *26*(1), 109–117. https://doi.org/10.1002/jqs.1438

Laberg, J. S., Stoker, M. S., Dahlgren, K. I. T., Haas, H. D., Haflidason, H., Hjelstuen, B. O., et al. (2005). Cenozoic alongslope processes and sedimentation on the NW European Atlantic margin. *Marine and Petroleum Geology*, *22*(9–10), 1069–1088. https://doi.org/10.1016/j.marpetgeo.2005.01.008

Landais, A., Capron, E., Masson-Delmotte, V., Toucanne, S., Rhodes, R., Popp, T., et al. (2018). Ice core evidence for decoupling between midlatitude atmospheric water cycle and Greenland temperature during the last deglaciation. *Climate of the Past*, *14*, 1405–1415. https://doi.org/10.5194/cp-14-1405-2018

Lehman, S. J., & Keigwin, L. D. (1992). Sudden changes in North Atlantic circulation during the last deglaciation. *Nature*, *356*(6372), 757–762. https://doi.org/10.1038/356757a0

Lekens, W. A. H., Haflidason, H., Sejrup, H. P., Nygard, A., Richter, T., Vogt, C., & Frederichs, T. (2009). Sedimentation history of the northern North Sea Margin during the last 150 ka. *Quaternary Science Reviews*, *28*(5–6), 469–483. https://doi.org/10.1016/j.quascirev.2008.11.010

Lekens, W. A. H., Sejrup, H. P., Haflidason, H., Knies, J., & Richter, T. (2006). Meltwater and ice rafting in the southern Norwegian Sea between 20 and 40 calendar kyr BP: Implications for Fennoscandian Heinrich events. *Paleoceanography*, *21*(3). https://doi.org/10.1029/2005pa001228

Li, C., Battisti, D. S., & Bitz, C. M. (2010). Can North Atlantic Sea ice anomalies account for Dansgaard-Oeschger climate signals?* *Journal of Climate*, *23*(20), 5457–5475. https://doi.org/10.1175/2010jcli3409.1

Li, C., Battisti, D. S., Schrag, D. P., & Tziperman, E. (2005). Abrupt climate shifts in Greenland due to displacements of the sea ice edge. *Geophysical Research Letters*, *32*(19). https://doi.org/10.1029/2005gl023492

Lincoln, P. C., Matthews, I. P., Palmer, A. P., Blockley, S. P., Staff, R. A., & Candy, I. (2020). Hydroclimatic changes in the British Isles through the last-glacial-interglacial transition: Multiproxy reconstructions from the Vale of Pickering, NE England. *Quaternary Science Reviews*, *249*, 106630. https://doi.org/10.1016/j.quascirev.2020.106630

Lippold, J., Luo, Y., Francois, R., Allen, S. E., Gherardi, J., Pichat, S., et al. (2012). Strength and geometry of the glacial Atlantic Meridional Overturning Circulation. *Nature Geoscience*, *5*(11), 813–816. https://doi.org/10.1038/ngeo1608

Liu, Z., Otto-Bliesner, B. L., He, F., Brady, E. C., Tomas, R., Clark, P. U., et al. (2009). Transient simulation of last deglaciation with a new mechanism for Bolling-Allerod Warming. *Science*, *325*(5938), 310–314. https://doi.org/10.1126/science.1171041

Löfverström, M., Caballero, R., Nilsson, J., & Kleman, J. (2014). Evolution of the large-scale atmospheric circulation in response to changing ice sheets over the last glacial cycle. *Climate of the Past*, *10*(4), 1453–1471. https://doi.org/10.5194/cp-10-1453-2014

Lozier, M. S., Li, F., Bacon, S., Bahr, F., Bower, A. S., Cunningham, S. A., et al. (2019). A sea change in our view of overturning in the subpolar North Atlantic. *Science*, *363*(6426), 516–521. https://doi.org/10.1126/science.aau6592

Lozier, M. S., & Stewart, N. M. (2008). On the temporally varying northward penetration of Mediterranean overflow water and eastward penetration of Labrador Sea Water. *Journal of Physical Oceanography*, *38*(9), 2097–2103. https://doi.org/10.1175/2008jpo3908.1

Lynch-Stieglitz, J. (2017). The Atlantic meridional overturning circulation and abrupt climate change. *Annual Review of Marine Science*, *9*, 83–104. https://doi.org/10.1146/annurev-marine-010816-060415

Lynch-Stieglitz, J., Adkins, J. F., Curry, W. B., Dokken, T., Hall, I. R., Herguera, J. C., et al. (2007). Atlantic meridional overturning circulation during the last glacial maximum. *Science*, *316*(5821), 66–69. https://doi.org/10.1126/science.1137127

Lynch-Stieglitz, J., Curry, W. B., & Slowey, N. (1999). Weaker Gulf Stream in the Florida straits during the last glacial maximum. *Nature*, *402*(6762), 644–648. https://doi.org/10.1038/45204

Lynch-Stieglitz, J., Schmidt, M. W., Gene Henry, L., Curry, W. B., Skinner, L. C., Mulitza, S., et al. (2014). Muted change in Atlantic overturning circulation over some glacial-aged Heinrich events. *Nature Geoscience*, *7*(2), 144–150. https://doi.org/10.1038/ngeo2045

Manabe, S., & Stouffer, R. J. (1995). Simulation of abrupt climate change induced by freshwater input to the North Atlantic Ocean. *Nature*, *378*(6553), 165–167. https://doi.org/10.1038/378165a0

Manighetti, B., & McCave, I. N. (1995). Late glacial and Holocene palaeocurrents around Rockall Bank, NE Atlantic Ocean. *Paleoceanography*, *10*(3), 611–626. https://doi.org/10.1029/94pa03059

Marchitto, T. M., & Broecker, W. S. (2006). Deep water mass geometry in the glacial Atlantic Ocean: A review of constraints from the paleonutrient proxy Cd/Ca. *Geochemistry, Geophysics, Geosystems*, *7*(12). https://doi.org/10.1029/2006gc001323

Marchitto, T. M., Curry, W. B., & Oppo, D. W. (1998). Millennial-scale changes in North Atlantic circulation since the last glaciation. *Nature*, *393*(6685), 557–561. https://doi.org/10.1038/31197

Marcott, S. A., Clark, P. U., Padman, L., Klinkhammer, G. P., Springer, S. R., Liu, Z., et al. (2011). Ice-shelf collapse from subsurface warming as a trigger for Heinrich events. *Proceedings of the National Academy of Sciences*, *108*(33), 13415–13419. https://doi.org/10.1073/pnas.1104772108

Marsh, R., Haigh, I. D., Cunningham, S. A., Inall, M. E., Porter, M., & Moat, B. I. (2017). Large-scale forcing of the European Slope Current and associated inflows to the North Sea. *Ocean Science*, *13*(2), 315–335. https://doi.org/10.5194/os-13-315-2017

McCave, I. N., & Andrews, J. T. (2019). Distinguishing current effects in sediments delivered to the ocean by ice. I. Principles, methods and examples. *Quaternary Science Reviews*, *212*, 92–107. https://doi.org/10.1016/j.quascirev.2019.03.031

McCave, I. N., Hall, I. R., Antia, A. N., Chou, L., Dehairs, F., Lampitt, R. S., et al. (2001). Distribution, composition and flux of particulate material over the European margin at 47°-50°N. *Deep Sea Research Part II: Topical Studies in Oceanography*, *48*(14–15), 3107–3139. https://doi.org/10.1016/s0967-0645(01)00034-0

McCave, I. N., Manighetti, B., & Beveridge, N. A. S. (1995). Circulation in the glacial North Atlantic inferred from grain-size measurements. *Nature*, *374*(6518), 149–152. https://doi.org/10.1038/374149a0

McCave, I. N., Manighetti, B., & Robinson, S. G. (1995). Sortable silt and fine sediment size/composition slicing: parameters for palaeocurrent speed and paleoceanography. *Paleoceanography*, *10*(3), 593–610. https://doi.org/10.1029/94pa03039

McCave, I. N., Thornalley, D. J. R., & Hall, I. R. (2017). Relation of sortable silt grain-size to deep-sea current speeds: Calibration of the 'Mud Current Meter'. *Deep Sea Research Part I: Oceanographic Research Papers*, *127*, 1–12. https://doi.org/10.1016/j.dsr.2017.07.003

McManus, J. F., Francois, R., Gherardi, J.-M., Keigwin, L. D., & Brown-Leger, S. (2004). Collapse and rapid resumption of Atlantic meridional circulation linked to deglacial climate changes. *Nature*, *428*(6985), 834–837. https://doi.org/10.1038/nature02494

Ménot, G., Bard, E., Rostek, F., Weijers, J. W. H., Hopmans, E. C., Schouten, S., & Damsté, J. S. S. (2006). Early reactivation of European rivers during the last deglaciation. *Science*, *313*(5793), 1623–1625. https://doi.org/10.1126/science.1130511

Menviel, L. C., Skinner, L. C., Tarasov, L., & Tzedakis, P. C. (2020). An ice–climate oscillatory framework for Dansgaard–Oeschger cycles. *Nature Reviews Earth & Environment*, *1*, 1–17.

Menviel, L., Timmermann, A., Friedrich, T., & England, M. H. (2014). Hindcasting the continuum of Dansgaard-Oeschger variability: Mechanisms, patterns and timing. *Climate of the Past*, *10*(1), 63. https://doi.org/10.5194/cp-10-63-2014

Mignot, J., Ganopolski, A., & Levermann, A. (2007). Atlantic subsurface temperatures: Response to a shutdown of the overturning circulation and consequences for its recovery. *Journal of Climate*, *20*(19), 4884–4898. https://doi.org/10.1175/jcli4280.1

Miramontes, E., Eggenhuisen, J. T., Jacinto, R. S., Poneti, G., Pohl, F., Normandeau, A., et al. (2020). Channel-levee evolution in combined contour current-turbidity current flows from flume-tank experiments. *Geology*, *48*(4), 353–357. https://doi.org/10.1130/g47111.1

Mojtahid, M., Toucanne, S., Fentimen, R., Barras, C., Le Houedec, S., Soulet, G., et al. (2017). Changes in northeast Atlantic hydrology during Termination 1: Insights from Celtic margin's benthic foraminifera. *Quaternary Science Reviews*, *175*, 45–59. https://doi.org/10.1016/j.quascirev.2017.09.003

Moros, M., Endler, R., Lackschewitz, K. S., Wallrabe-Adams, H.-J., Mienert, J., & Lemke, W. (1997). Physical properties of Reykjanes Ridge sediments and their linkage to high-resolution Greenland Ice Sheet Project 2 ice core data. *Paleoceanography*, *12*(5), 687–695. https://doi.org/10.1029/97pa02030

Mulder, T., Syvitski, J. P. M., Migeon, S., Faugères, J.-C., & Savoye, B. (2003). Marine hyperpycnal flows: initiation, behavior and related deposits. A review. *Marine and Petroleum Geology*, *20*(6–8), 861–882. https://doi.org/10.1016/j.marpetgeo.2003.01.003

Naughton, F., Sánchez Goñi, M. F., Kageyama, M., Bard, E., Duprat, J., Cortijo, E., et al. (2009). Wet to dry climatic trend in north-western Iberia within Heinrich events. *Earth and Planetary Science Letters*, *284*(3–4), 329–342. https://doi.org/10.1016/j.epsl.2009.05.001

Ng, H. C., Robinson, L. F., McManus, J. F., Mohamed, K. J., Jacobel, A. W., Ivanovic, R. F., et al. (2018). Coherent deglacial changes in western Atlantic Ocean circulation. *Nature Communications*, *9*(1), 1–10. https://doi.org/10.1038/s41467-018-05312-3

O'Cofaigh, C., Weilbach, K., Lloyd, J. M., Benetti, S., Callard, S. L., Purcell, C., et al. (2019). Early deglaciation of the British-Irish Ice Sheet on the Atlantic shelf northwest of Ireland driven by glacioisostatic depression and high relative sea level. *Quaternary Science Reviews*, *208*, 76–96.

Oppo, D. W., & Lehman, S. J. (1993). Mid-depth circulation of the subpolar North Atlantic during the last glacial maximum. *Science*, *259*(5098), 1148–1152. https://doi.org/10.1126/science.259.5098.1148

Orvik, K. A., & Niiler, P. (2002). Major pathways of Atlantic water in the northern North Atlantic and Nordic Seas toward Arctic. *Geophysical Research Letters*, *29*(19), 2–1. https://doi.org/10.1029/2002gl015002

Otto-Bliesner, B. L., Brady, E. C., Clauzet, G., Tomas, R., Levis, S., & Kothavala, Z. (2006). Last glacial maximum and Holocene climate in CCSM3. *Journal of Climate*, *19*(11), 2526–2544. https://doi.org/10.1175/jcli3748.1

Patton, H., Hubbard, A., Andreassen, K., Auriac, A., Whitehouse, P. L., Stroeven, A. P., et al. (2017). Deglaciation of the Eurasian ice sheet complex. *Quaternary Science Reviews*, *169*, 148–172. https://doi.org/10.1016/j.quascirev.2017.05.019

Pausata, F. S. R., Li, C., Wettstein, J. J., Kageyama, M., & Nisancioglu, K. H. (2011). The key role of topography in altering North Atlantic atmospheric circulation during the last glacial period. *Climate of the Past*, *7*(4), 1089–1101. https://doi.org/10.5194/cp-7-1089-2011

Peck, V. L., Hall, I. R., Zahn, R., Elderfield, H., Grousset, F., Hemming, S. R., & Scourse, J. D. (2006). High resolution evidence for linkages between NW European ice sheet instability and Atlantic Meridional Overturning Circulation. *Earth and Planetary Science Letters*, *243*(3–4), 476–488. https://doi.org/10.1016/j.epsl.2005.12.023

Peck, V. L., Hall, I. R., Zahn, R., Grousset, F., Hemming, S. R., & Scourse, J. D. (2007). The relationship of Heinrich events and their European precursors over the past 60ka BP: A multi-proxy ice-rafted debris provenance study in the North East Atlantic. *Quaternary Science Reviews*, *26*(7–8), 862–875. https://doi.org/10.1016/j.quascirev.2006.12.002

Peck, V. L., Hall, I. R., Zahn, R., & Scourse, J. D. (2007). Progressive reduction in NE Atlantic intermediate water ventilation prior to Heinrich events: Response to NW European ice sheet instabilities? *Geochemistry, Geophysics, Geosystems*, *8*(1). https://doi.org/10.1029/2006gc001321

Peltier, W. R., & Vettoretti, G. (2014). Dansgaard-Oeschger oscillations predicted in a comprehensive model of glacial climate: A "kicked" salt oscillator in the Atlantic. *Geophysical Research Letters*, *41*(20), 7306–7313. https://doi.org/10.1002/2014gl061413

Petersen, S. V., Schrag, D. P., & Clark, P. U. (2013). A new mechanism for Dansgaard-Oeschger cycles. *Paleoceanography*, *28*(1), 24–30. https://doi.org/10.1029/2012pa002364

Pflaumann, U., Sarnthein, M., Chapman, M., d'Abreu, L., Funnell, B., Huels, M., et al. (2003). Glacial North Atlantic: Sea-surface conditions reconstructed by GLAMAP 2000. *Paleoceanography*, *18*(3). https://doi.org/10.1029/2002pa000774

Pingree, R. D., & Le Cann, B. (1989). Celtic and Armorican slope and shelf residual currents. *Progress in Oceanography*, *23*(4), 303–338. https://doi.org/10.1016/0079-6611(89)90003-7

Pingree, R. D., & Le Cann, B. (1990). Structure, strength and seasonality of the slope currents in the Bay of Biscay region. *Journal of the Marine Biological Association*, *70*(4), 857–885. https://doi.org/10.1017/s0025315400059117

Pingree, R. D., Sinha, B., & Griffiths, C. R. (1999). Seasonality of the European slope current (Goban Spur) and ocean margin exchange. *Continental Shelf Research*, *19*(7), 929–975. https://doi.org/10.1016/s0278-4343(98)00116-2

Pöppelmeier, F., Blaser, P., Gutjahr, M., Jaccard, S. L., Frank, M., Max, L., & Lippold, J. (2020). Northern-sourced water dominated the Atlantic Ocean during the Last Glacial Maximum. *Geology*, *48*(8), 826–829. https://doi.org/10.1130/g47628.1

Praetorius, S. K., McManus, J. F., Oppo, D. W., & Curry, W. B. (2008). Episodic reductions in bottom-water currents since the last ice age. *Nature Geoscience*, *1*(7), 449–452. https://doi.org/10.1038/ngeo227

Rahmstorf, S. (2002). Ocean circulation and climate during the past 120,000 years. *Nature*, *419*(6903), 207–214. https://doi.org/10.1038/nature01090

Rasmussen, S. O., Andersen, K. K., Svensson, A. M., Steffensen, J. P., Vinther, B. M., Clausen, H. B., et al. (2006). A new Greenland ice core chronology for the last glacial termination. *Journal of Geophysical Research*, *111*(D6). https://doi.org/10.1029/2005jd006079

Rasmussen, S. O., Bigler, M., Blockley, S. P., Blunier, T., Buchardt, S. L., Clausen, H. B., et al. (2014). A stratigraphic framework for abrupt climatic changes during the Last Glacial period based on three synchronized Greenland ice-core records: refining and extending the INTIMATE event stratigraphy. *Quaternary Science Reviews*, *106*, 14–28. https://doi.org/10.1016/j.quascirev.2014.09.007

Rasmussen, T. L., & Thomsen, E. (2004). The role of the North Atlantic Drift in the millennial timescale glacial climate fluctuations. *Palaeogeography, Palaeoclimatology, Palaeoecology*, *210*(1), 101–116. https://doi.org/10.1016/j.palaeo.2004.04.005

Rasmussen, T. L., & Thomsen, E. (2008). Warm Atlantic surface water inflow to the Nordic seas 34–10 calibrated ka BP. *Paleoceanography*, *23*(1). https://doi.org/10.1029/2007pa001453

Rasmussen, T. L., & Thomsen, E. (2009). Ventilation changes in intermediate water on millennial time scales in the SE Nordic seas, 65-14 kyr BP. *Geophysical Research Letters*, *36*(1). https://doi.org/10.1029/2008gl036563

Rasmussen, T. L., Thomsen, E., van Weering, T. C. E., & Labeyrie, L. (1996). Rapid changes in surface and deep water conditions at the Faeroe Margin during the last 58,000 years. *Paleoceanography*, *11*(6), 757–771. https://doi.org/10.1029/96pa02618

Roberts, N. L., & Piotrowski, A. M. (2015). Radiogenic Nd isotope labeling of the northern NE Atlantic during MIS 2. *Earth and Planetary Science Letters*, *423*, 125–133. https://doi.org/10.1016/j.epsl.2015.05.011

Roche, D. M., Wiersma, A. P., & Renssen, H. (2010). A systematic study of the impact of freshwater pulses with respect to different geographical locations. *Climate Dynamics*, *34*(7–8), 997–1013. https://doi.org/10.1007/s00382-009-0578-8

Rogerson, M., Rohling, E. J., Bigg, G. R., & Ramirez, J. (2012). Paleoceanography of the Atlantic-Mediterranean exchange: Overview and first quantitative assessment of climatic forcing. *Reviews of Geophysics*, *50*(2). https://doi.org/10.1029/2011rg000376

Rothwell, R. G., & Croudace, I. W. (2015). Twenty years of XRF core scanning marine sediments: what do geochemical proxies tell us? In *Micro-XRF studies of sediment cores* (pp. 25–102). Netherlands: Springer

Sadatzki, H., Dokken, T. M., Berben, S. M., Muschitiello, F., Stein, R., Fahl, K., et al. (2019). Sea ice variability in the southern Norwegian Sea during glacial Dansgaard-Oeschger climate cycles. *Science Advances*, *5*(3), eaau6174. https://doi.org/10.1126/sciadv.aau6174

Saha, R. (2015). Millennial-scale oscillations between sea ice and convective deep water formation. *Paleoceanography*, *30*(11), 1540–1555. https://doi.org/10.1002/2015pa002809

Sarafanov, A., Falina, A., Mercier, H., Sokov, A., Lherminier, P., Gourcuff, C., et al. (2012). Mean full-depth summer circulation and transports at the northern periphery of the Atlantic Ocean in the 2000s. *Journal of Geophysical Research*, *117*(C1). https://doi.org/10.1029/2011jc007572

Sarnthein, M., Winn, K., Jung, S. J. A., Duplessy, J.-C., Labeyrie, L., Erlenkeuser, H., & Ganssen, G. (1994). Changes in east Atlantic deepwater circulation over the last 30,000 years: Eight time slice reconstructions. *Paleoceanography*, *9*(2), 209–267. https://doi.org/10.1029/93pa03301

Scourse, J. D., Haapaniemi, A. I., Colmenero-Hidalgo, E., Peck, V. L., Hall, I. R., Austin, W. E. N., et al. (2009). Growth, dynamics and deglaciation of the last British-Irish ice sheet: the deep-sea ice-rafted detritus record. *Quaternary Science Reviews*, *28*(27–28), 3066–3084. https://doi.org/10.1016/j.quascirev.2009.08.009

Scourse, J. D., Hall, I. R., McCave, I. N., Young, J. R., & Sugdon, C. (2000). The origin of Heinrich layers: evidence from H2 for European precursor events. *Earth and Planetary Science Letters*, *182*(2), 187–195. https://doi.org/10.1016/s0012-821x(00)00241-7

Sévellec, F., & Fedorov, A. V. (2015). Unstable AMOC during glacial intervals and millennial variability: The role of mean sea ice extent. *Earth and Planetary Science Letters*, *429*, 60–68. https://doi.org/10.1016/j.epsl.2015.07.022

Shaffer, G., Olsen, S. M., & Bjerrum, C. J. (2004). Ocean subsurface warming as a mechanism for coupling Dansgaard-Oeschger climate cycles and ice-rafting events. *Geophysical Research Letters*, *31*(24). https://doi.org/10.1029/2004gl020968

Siddall, M., Khatiwala, S., van de Flierdt, T., Jones, K., Goldstein, S. L., Hemming, S., & Anderson, R. F. (2008). Toward explaining the Nd paradox using reversible scavenging in an ocean general circulation model. *Earth and Planetary Science Letters*, *274*(3–4), 448–461. https://doi.org/10.1016/j.epsl.2008.07.044

Small, D., Smedley, R. K., Chiverrell, R. C., Scourse, J. D., Cofaigh, C. Ó., Duller, G. A. T., et al. (2018). Trough geometry was a greater influence than climate-ocean forcing in regulating retreat of the marine-based Irish-Sea Ice Stream. *GSA Bulletin*, *130*(11–12), 1981–1999. https://doi.org/10.1130/b31852.1

Smedley, R. K., Chiverrell, R. C., Ballantyne, C. K., Burke, M. J., Clark, C. D., Duller, G. A. T., et al. (2017). Internal dynamics condition centennial-scale oscillations in marine-based ice-stream retreat. *Geology*, *45*(9), 787–790. https://doi.org/10.1130/g38991.1

Smedley, R. K., Scourse, J. D., Small, D., Hiemstra, J. F., Duller, G. A. T., Bateman, M. D., et al. (2017). New age constraints for the limit of the British-Irish Ice Sheet on the Isles of Scilly. *Journal of Quaternary Science*, *32*(1), 48–62. https://doi.org/10.1002/jqs.2922

Stow, D. A. V., & Holbrook, J. A. (1984). North Atlantic contourites: an overview. *Geological Society, London, Special Publications*, *15*(1), 245–256. https://doi.org/10.1144/gsl.sp.1984.015.01.16

Svensson, A., Andersen, K. K., Bigler, M., Clausen, H. B., Dahl-Jensen, D., Davies, S. M., et al. (2008). A 60 000 year Greenland stratigraphic ice core chronology. *Climate of the Past*, *4*, 47–57. https://doi.org/10.5194/cp-4-47-2008

Tachikawa, K., Piotrowski, A. M., & Bayon, G. (2014). Neodymium associated with foraminiferal carbonate as a recorder of seawater isotopic signatures. *Quaternary Science Reviews*, *88*, 1–13. https://doi.org/10.1016/j.quascirev.2013.12.027

Tanaka, T., Togashi, S., Kamioka, H., Amakawa, H., Kagami, H., Hamamoto, T., et al. (2000). JNdi-1: A neodymium isotopic reference in consistency with LaJolla neodymium. *Chemical Geology*, *168*(3–4), 279–281. https://doi.org/10.1016/s0009-2541(00)00198-4

Thomsen, L., & Van Weering, T. C. E. (1998). Spatial and temporal variability of particulate matter in the benthic boundary layer at the N.W. European Continental Margin (Goban Spur). *Progress in Oceanography*, *42*(1–4), 61–76. https://doi.org/10.1016/s0079-6611(98)00028-7

Thornalley, D. J. R., Barker, S., Becker, J., Hall, I. R., & Knorr, G. (2013). Abrupt changes in deep Atlantic circulation during the transition to full glacial conditions. *Paleoceanography*, *28*(2), 253–262. https://doi.org/10.1002/palo.20025

Thornalley, D. J. R., Bauch, H. A., Gebbie, G., Guo, W., Ziegler, M., Bernasconi, S. M., et al. (2015). A warm and poorly ventilated deep Arctic Mediterranean during the last glacial period. *Science*, *349*(6249), 706–710. https://doi.org/10.1126/science.aaa9554

Toucanne, S., Mulder, T., Schönfeld, J., Hanquiez, V., Gonthier, E., Duprat, J., et al. (2007). Contourites of the Gulf of Cadiz: A high-resolution record of the paleocirculation of the Mediterranean outflow water during the last 50,000 years. *Palaeogeography, Palaeoclimatology, Palaeoecology*, *246*(2–4), 354–366. https://doi.org/10.1016/j.palaeo.2006.10.007

Toucanne, S., Soulet, G., Freslon, N., Silva Jacinto, R., Dennielou, B., Zaragosi, S., et al. (2015). Millennial-scale fluctuations of the European Ice Sheet at the end of the last glacial, and their potential impact on global climate. *Quaternary Science Reviews*, *123*, 113–133. https://doi.org/10.1016/j.quascirev.2015.06.010

Toucanne, S., Zaragosi, S., Bourillet, J.-F., Marieu, V., Cremer, M., Kageyama, M., et al. (2010). The first estimation of Fleuve Manche palaeoriver discharge during the last deglaciation: Evidence for Fennoscandian ice sheet meltwater flow in the English Channel ca 20-18ka ago. *Earth and Planetary Science Letters*, *290*, 459–473. https://doi.org/10.1016/j.epsl.2009.12.050

Toyos, M. H., Lamy, F., Lange, C. B., Lembke-Jene, L., Saavedra-Pellitero, M., Esper, O., & Arz, H. W. (2020). Antarctic Circumpolar Current dynamics at the Pacific entrance to the Drake Passage over the past 1.3 million years. *Paleoceanography and Paleoclimatology*, *35*(7), e2019PA003773. https://doi.org/10.1029/2019pa003773

Trenberth, K. E., Zhang, Y., Fasullo, J. T., & Cheng, L. (2019). Observation-based estimates of global and basin ocean meridional heat transport time series. *Journal of Climate*, *32*(14), 4567–4583. https://doi.org/10.1175/jcli-d-18-0872.1

Van Aken, H. M. (2000). The hydrography of the mid-latitude Northeast Atlantic Ocean. *Deep Sea Research Part I: Oceanographic Research Papers*, *47*(5), 789–824. https://doi.org/10.1016/s0967-0637(99)00112-0

Vautravers, M. J., Shackleton, N. J., Lopez-Martinez, C., & Grimalt, J. O. (2004). Gulf Stream variability during marine isotope stage 3. *Paleoceanography*, *19*(2). https://doi.org/10.1029/2003pa000966

Vettoretti, G., & Peltier, W. R. (2013). Last Glacial Maximum ice sheet impacts on North Atlantic climate variability: The importance of the sea ice lid. *Geophysical Research Letters*, *40*(24), 6378–6383. https://doi.org/10.1002/2013gl058486

Voelker, A., Lebreiro, S., Schönfeld, J., Cacho, I., Erlenkeuser, H., & Abrantes, F. (2006). Mediterranean outflow strengthening during northern hemisphere coolings: A salt source for the glacial Atlantic? *Earth and Planetary Science Letters*, *245*(1–2), 39–55. https://doi.org/10.1016/j.epsl.2006.03.014

Waelbroeck, C., Lougheed, B. C., Riveiros, N. V., Missiaen, L., Pedro, J., Dokken, T., et al. (2019). Consistently dated Atlantic sediment cores over the last 40 thousand years. *Scientific Data*, *6*(1), 1–12.

Waelbroeck, C., Pichat, S., Böhm, E., Lougheed, B. C., Faranda, D., Vrac, M., et al. (2018). Relative timing of precipitation and ocean circulation changes in the western equatorial Atlantic over the last 45 kyr. *Climate of the Past*, *14*(9), 1315–1330. https://doi.org/10.5194/cp-14-1315-2018

WAIS Divide Project Members. (2015). Precise interpolar phasing of abrupt climate change during the last ice age. *Nature*, *520*(7549), 661.

Wary, M., Eynaud, F., Swingedouw, D., Masson-Delmotte, V., Matthiessen, J., Kissel, C., et al. (2017). Regional seesaw between the North Atlantic and Nordic Seas during the last glacial abrupt climate events. *Climate of the Past*, *13*(6), 729–739. https://doi.org/10.5194/cp-13-729-2017

Webb, R. S., Rind, D. H., Lehman, S. J., Healy, R. J., & Sigman, D. (1997). Influence of ocean heat transport on the climate of the Last Glacial Maximum. *Nature*, *385*(6618), 695–699. https://doi.org/10.1038/385695a0

Weber, S. L., Drijfhout, S. S., Abe-Ouchi, A., Crucifix, M., Eby, M., Ganopolski, A., et al. (2007). The modern and glacial overturning circulation in the Atlantic Ocean in PMIP coupled model simulations. *Climate of the Past*, *3*, 51–64. https://doi.org/10.5194/cp-3-51-2007

Weinelt, M., Vogelsang, E., Kucera, M., Pflaumann, U., Sarnthein, M., Voelker, A., et al. (2003). Variability of North Atlantic heat transfer during MIS 2. *Paleoceanography*, *18*(3). https://doi.org/10.1029/2002pa000772

Weltje, G. J., & Tjallingii, R. (2008). Calibration of XRF core scanners for quantitative geochemical logging of sediment cores: Theory and application. *Earth and Planetary Science Letters*, *274*(3–4), 423–438. https://doi.org/10.1016/j.epsl.2008.07.054

Willamowski, C., & Zahn, R. (2000). Upper ocean circulation in the glacial North Atlantic from benthic foraminiferal isotope and trace element fingerprinting. *Paleoceanography*, *15*(5), 515–527. https://doi.org/10.1029/1999pa000467

Wu, L., Wilson, D. J., Wang, R., Yin, X., Chen, Z., Xiao, W., & Huang, M. (2020). Evaluating Zr/Rb ratio from XRF scanning as an indicator of grain-size variations of glaciomarine sediments in the Southern Ocean. *Geochemistry, Geophysics, Geosystems*, *21*(11), e2020GC009350

Wunsch, C. (2006). Abrupt climate change: An alternative view. *Quaternary Research*, *65*(2), 191–203. https://doi.org/10.1016/j.yqres.2005.10.006

Xu, W., Miller, P. I., Quartly, G. D., & Pingree, R. D. (2015). Seasonality and interannual variability of the European Slope Current from 20 years of altimeter data compared with in situ measurements. *Remote Sensing of Environment*, *162*, 196–207. https://doi.org/10.1016/j.rse.2015.02.008

Zahn, R., Schönfeld, J., Kudrass, H.-R., Park, M.-H., Erlenkeuser, H., & Grootes, P. (1997). Thermohaline instability in the North Atlantic during meltwater events: Stable isotope and ice-rafted detritus records from Core SO75-26KL, Portuguese Margin. *Paleoceanography*, *12*(5), 696–710. https://doi.org/10.1029/97pa00581

Zahn, R., & Stüber, A. (2002). Suborbital intermediate water variability inferred from paired benthic foraminiferal Cd/Ca and δ13C in the tropical West Atlantic and linking with North Atlantic climates. *Earth and Planetary Science Letters*, *200*(1–2), 191–205. https://doi.org/10.1016/s0012-821x(02)00613-1

Zaragosi, S., Eynaud, F., Pujol, C., Auffret, G. A., Turon, J.-L., & Garlan, T. (2001). Initiation of the European deglaciation as recorded in the northwestern Bay of Biscay slope environments (Meriadzek Terrace and Trevelyan Escarpment): a multi-proxy approach. *Earth and Planetary Science Letters*, *188*(3–4), 493–507. https://doi.org/10.1016/s0012-821x(01)00332-6

Zhang, X., Knorr, G., Lohmann, G., & Barker, S. (2017). Abrupt North Atlantic circulation changes in response to gradual CO2 forcing in a glacial climate state. *Nature Geoscience*, *10*(7), 518–523. https://doi.org/10.1038/ngeo2974

Zhang, X., Lohmann, G., Knorr, G., & Purcell, C. (2014). Abrupt glacial climate shifts controlled by ice sheet changes. *Nature*, *512*(7514), 290–294. https://doi.org/10.1038/nature13592

Zhang, X., & Prange, M. (2020). Stability of the Atlantic overturning circulation under intermediate (MIS3) and full glacial (LGM) conditions and its relationship with Dansgaard-Oeschger climate variability. *Quaternary Science Reviews*, *242*, 106443. https://doi.org/10.1016/j.quascirev.2020.106443

Zou, S., Lozier, S., Zenk, W., Bower, A., & Johns, W. (2017). Observed and modeled pathways of the Iceland Scotland Overflow Water in the eastern North Atlantic. *Progress in Oceanography*, *159*, 211–222. https://doi.org/10.1016/j.pocean.2017.10.003